[redacted]

Second Semiannual Progress Report
to
The National Aeronautics and Space Administration
on
The TM Project

"UTILIZING REMOTE SENSING OF THEMATIC MAPPER DATA TO IMPROVE OUR UNDERSTANDING OF ESTUARINE PROCESSES AND THEIR INFLUENCE ON THE PRODUCTIVITY OF ESTUARINE-DEPENDENT FISHERIES"

Joan A. Browder
Miami, Fla., Unit of Beaufort, N.C., Laboratory
Southeast Fisheries Center
Miami, FL 33149

NJ580778

L. Nelson May, Jr.
Coastal Fisheries Institute
Center for Wetland Resources
Louisiana State University
Baton Rouge, LA 70803

L5232337

Alan Rosenthal
Miami, Fla., Unit of Beaufort, N.C., Laboratory
Southeast Fisheries Center
Miami, FL 33149

NJ580778

Robert H. Baumann
Center for Energy Studies
Louisiana State University
Baton Rouge, LA 70803

L5232337

James G. Gosselink
Coastal Ecology Institute
Center for Wetland Resources
Louisiana State University
Baton Rouge, LA 70803

L5232337

June 10, 1986

INTRODUCTION

Landsat thematic mapper (TM) data are being used to refine and validate a stochastic spatial computer model to be applied to coastal resource management problems in Louisiana. Two major aspects of the research are:

1. The measurement of area of land (or emergent vegetation) and water and the length of the interface between land and water in TM imagery of selected coastal wetlands (sample marshes) and;
2. The comparison of spatial patterns of land and water in the sample marshes of the imagery to that in marshes simulated by the computer model.

Two research teams are involved in the project. The first is at the Southeast Fisheries Center of the National Marine Fisheries Service in Miami (Miami Unit of the Beaufort, North Carolina, laboratory). The second is at Louisiana State University's Center for Wetland Resources and Center for Energy Studies in Baton Rouge.

The primary activity of the NMFS team during the first year of the project has been to develop and test parameters to use in comparing spatial patterns. An exploration of several parameters devised for use in this project were discussed in the first semiannual progress report. The potential use of a published autocorrelation statistic will be analyzed in the present report. Activity at LSU during the first nine months of the project (the project started three months later at LSU than at NMFS) has involved selecting imagery of sample marshes, preparing the selected images for analysis, evaluating techniques for use in classifying land and water pixels in the imagery, and testing the accuracy of the image processing software in measuring length of the land-water interface on digital maps in which land and water are clearly distinguished.

First, we will present the NMFS work with the autocorrelation statistics, then the LSU work with the model.

NMFS ACTIVITIES

A stochastic spatial simulation model was developed by Browder et al. (1985a) to determine the theoretical relationship between the length of the interface between land and water and the loss of marshland through conversion of land to water. To validate this model, we plan to compare model-simulated patterns of land and water with those of actual marshes, as interpreted from thematic mapper imagery. We are investigating the measurement of spatial autocorrelation as a means of comparing the simulated patterns with the imagery.

Starting with solid land, the model simulates the disintegration of the marsh one pixel at a time until nothing is left but open water. The specific pixel that converts from land to water at each iteration is determined by a probability function linked to a random-number generator. Weighting-factor coefficients in the probability function can be adjusted to affect the probability that a given pixel will disintegrate at the next iteration according to its initial location in the marsh relative to the main water body (weighting factor G) and according to the number of sides on which it is bordered by water (weighting factor W). Weighting factors affect the pattern of land and water in the simulated marsh at its various stages of disintegration.

A spatial map possesses the property of autocorrelation if it contains values that exhibit an organized pattern. Such an organization may arise if the value assigned to a location is to some extent influenced by values assigned to neighboring locations. Without influence from other than random processes, a spatial map lacks spatial autocorrelation.

Since weighting factors determine the degree of influence of neighboring locations, it seems likely that they determine the degree of autocorrelation in the resulting land-water pattern. Measuring autocorrelation in actual marshes might, therefore, allow us to approximate the spatial patterns of the actual marshes with model simulations, if we can determine the relationship between an autocorrelation measure and the weighting factors of the model.

Various measures of spatial autocorrelation in the plane and their corresponding random variables have been defined (Cliff and Ord 1981, Upton and Fingleton 1985). Approximate tests of significance for systematic variation in spatial patterns can be performed by evaluating these variables as standard normal deviates. In the present study, which uses binary (0,1) spatial data from a simulation model, the general cross-product statistic, R, and the corresponding random variables, the expected value of R, E(R), and the variance of R, var(R), were used to assess the spatial organization of simulated patterns produced by weighting factors ranging from W=Ø to W=76 with G=W (set 1) and, alternatively, G=Ø for all W (set 2). Various sensitivity tests were performed to examine the regularity of the behavior of these variables. Results of our analysis show how the cross-product statistic and its corresponding random variables change with weighting factor and with the overall size of the spatial sample (number of pixels), its configuration (columns/rows), and the level of disintegration (water pixels as a percentage of total pixels).

We applied curve-fitting techniques to the autocorrelation data from the sensitivity tests to formulate regression equations that predict R under different combinations of conditions. These equations, when more fully developed, will serve as a conduit between the analyzed imagery and

model simulations. The autocorrelative properties of specific wetland areas will first be determined and then channeled into the predictive equations to determine how weighting factors should be set. Spatial patterns possessing approximately the same degree of autocorrelation as the actual TM spatial patterns can then be simulated. More refined comparisons between the actual and simulated marsh can then be made to ensure that the two are indeed similar. Comparisons to be made include frequency distribution of pixels by water-body size, frequency distribution of water pixels by numbers of sides bordered by water, and percentage of water pixels with distance from the main water body (Browder et al. 1985b).

Assigning weighting factors to actual marshes via the above procedure will allow us to place these marshes on theoretical trajectories of change in land-water interface, as determined by model-simulations of marsh disintegration. If we can find several sample marshes in different stages of disintegration that fit on the same theoretical trajectory of change, then we can compare the actual interface to the theoretical interface at each disintegration stage. Conformity of actual to simulated change in interface will not only validate the model, but will also allow us to predict the rate and direction of future change in interface in each of the sample marshes with respect to rate of marsh disintegration.

Description of the Experiments

A new version of the model was written in Fortran 77 and implemented on a 32-bit Burroughs 6800 mini computer. Two more algorithms were added. The first calculated the expected value and variance of the general cross-product statistic for spatial matrices of various sizes, configurations, and levels of disintegration. The second determined the

general cross-product statistic of land-water pattern in 30 simulated marshes disintegrated to the same level and produced by the same weighting factors. For later comparisons, the mean and variance of R were calculated for these 30 replications.

Test of the Random Number Generator

The model utilized the Burrough's mixed congruential random-number generator. In order to determine the quality of the random-number generator for generating random sequences, we tested uniformity with the chi-square goodness-of-fit test (Fishman 1973). We collected 65,541 random numbers on a run and divided the unit interval into 4,096 equal subintervals so that, according to the hypothesis of uniformity, the probability that a number fell into a particular interval was 1/4,096, and the expected number of observations in a particular interval was about 16. On this binary machine, the choice of 4,096 ($4{,}096 = 2^{12}$) allowed us to test the 12 most significant bits. Table 1 shows the results for 10 independent executions. The largest chi-square value occurred on execution 7, and, since the normalized deviate of this value is less than the point on the cumulative normal curve corresponding to probability 0.05, we accepted the hypothesis of uniformity of each of the 10 executions at the 0.05 level.

As a further test of the integrity of the random-number generator, a runs-up-and-down test was employed to determine whether a sequence of 30 general cross-product statistics was generated by a random process. A two-sided test was set up with the alpha risk controlled at 0.01. Table 2 shows the results for 10 independent executions. For each of the executions, the test statistic, which is a count of the number of changes of direction between consecutive numbers in a sequence, did not exceed

the cutoff points on the normal curve. We, therefore, concluded that the sequence was generated by a random process.

The General Cross-product Statistic

The general cross-product statistic is given by equation (1):

$$R = \Sigma_i \Sigma_j W_{ij} Y_{ij} \qquad (1)$$

W_{ij} is a proximity value with $W_{ij} = 1$ if locations in the spatial matrix are contiguous and $W_{ij} = 0$ otherwise. $Y_{ij} = (x_i - x_j)^2$, where x_i and x_j are the observed values at locations i and j. In our case these values also are either 1 or 0.

Equations (2) and (3) give the expected value and variance of R.

$$E(R) = S_o T_o / n(n-1) \qquad (2)$$

$$\text{var}(R) = \qquad (3)$$

$$\frac{S_1 T_1}{2n(^2)} + \frac{(S_2 - 2S_1)(T_2 - 2T_1)}{4n(^3)} + \frac{(S_0^2 + S_1 - S_2)(T_0^2 + T_1 - T_2)}{n(^4)} - [E(R)]$$

where

$So = \Sigma_i \Sigma_j W_{ij}$ $(i \neq j)$; $S_1 = \frac{1}{2}\Sigma_i \Sigma_j (W_{ij} + W_{ji})^2$ $(i \neq j)$; $S_2 = \Sigma_i (W_{io} + W_{oi})^2$

$W_{io} = \Sigma_j W_{ij}$; $W_{oi} = \Sigma_j W_{ji}$; $n(^2) = n(n-1)$; $n(^3) = n(n-1)(n-2)$; $n(^4) = n(n-1)(n-2)(n-3)$

Sensitivity Tests

One set of replicates of simulated patterns was generated by setting the G weighting factor (initial adjacency to main water body) equal to the W weighting factor (adjacency to water), and a second set was generated by setting the G weighting factor at zero. The first situation assumes that the marsh is bordered on one side by water and on the other three sides by land. The second assumes that the marsh is bordered on all four sides by land. Marshes that lie somewhat inland from the main water body probably fall somewhere in between these two extremes.

Matrices were constructed that contained 1,000, 800, 600, 400, 200, and 100 pixels each. For each of these matrix sizes, R-mean was calculated for all combinations of levels of disintegration (0.1, 0.2, 0.3, 0.4, 0.5) and weighting factors (set 1: 0,0; 4,4; 8,8; 12,12; 24,24; 76,76; set 2: 0,0; 4,0; 8,0; 12,0; 24,0; 76,0). The results from set 1 in appendix Tables 1-6 and those from set 2 in appendix Tables 7-12 show R-mean and sample variance and the corresponding random variables, E(R) and var(R).

According to the Z-test statistic, the R-means generated from weighting factors set at zero were not significantly different from the corresponding E(R) (alpha = 0.05), indicating the absence of autocorrelation. R-means for spatial patterns simulated with weighting factors set at 4,4 or 4,0 or greater were significantly different from E(R) (alpha = 0.001), demonstrating that weighting factors cause autocorrelation in the spatial patterns of land and water simulated by the model and that the autocorrelation caused by the weighting factor can be detected as a difference between the R-mean and E(R).

The sample variances of R-means generated with weighting factors set at zero appeared considerably different from var(R), but only three out of the 34 sample variances in appendix Tables 7-12 were significantly different according to the chi-square test statistic

$$X_2 = \frac{(n-1)\ S^2}{\sigma^2} \qquad (4)$$

from Beaver and Mendenhall (1971).

Figures 1-12 show how R-mean changes as a function of weighting factors and level of disintegration for each matrix size in each of the sets. R-mean decreased with increasing weighting factor and varied with matrix size and level of disintegration. Plots of R-mean for each of the sets reveal separate curves for each level of disintegration--a family of curves that has the following characteristics: (1) R-means that decline rapidly with increased weighting factors in the low range of weighting factors but more gradually in the higher range of weighting factors; and (2) R-mean values that are lower at lower levels of disintegration and decline more gradually in the lower range of weighting factor than do those at higher disintegration levels.

The cross-product statistic and its random variants vary similarly with level of disintegration on both sides of disintegration level 0.5. This can best be seen in Figure 13, a plot of E(R) with level. The plotted values are shown in Table 3. Table 4 shows that var(R) varies similarly with level. Tables 5 and 6 show R-means and sample variance for 1,000-pixel marshes produced by set-1 weighting factors at levels of disintegration from 0.1 through 0.9. E(R)'s for 1,000-pixel marshes at the nine levels of disintegration are also shown. Both R-mean and E(R)

are almost identical for levels 0.6 and 0.4, levels 0.7 and 0.3, levels 0.8 and 0.2, and levels 0.9 and 0.1.

The cross-product statistic and its random variants increase linearly with marsh size; however, the relationship is slightly confounded by the effects of configuration (the ratio of rows to columns). Figure 14 shows linear relationships between E(R) and marsh size when configuration is held constant at 1, 2, and 4. There are three distinct lines that do not have exactly the same slope. The relationship of var(R) to marsh size differs similarly with configuration (Figure 15). A straight-line relationship is obtained even when configuration is not held constant; however, it might be difficult to use such a relationship predictively to extrapolate E(R) for matrix sizes beyond the range of the data. That configuration affects E(R) is further demonstrated in Table 7, which shows E(R) at the 0.5 level of disintegration for pairs of matrices having the same number of pixels but different configurations. Paired matrices are 10 x 2n and 20 x n; n = 5, 10, 20, 30, 40, or 50. Of the six pairs of matrices, only the 10 x 20 (ratio 0.5) matrix and 20 x 10 (ratio 2.0) matrix have the same E(R). Apparently inverse configurations are identical as far as E(R) is concerned. The values plotted in Figure 14 and 15 were taken from Tables 7 and 8.

Predictive Equations

A curve-fitting technique was used to develop equations for the relationship of R to weighting factor and the effect of level of disintegration. The data inputs were R-mean values for a 1,000-pixel (20 x 50) matrix produced with set-1 weighting factors. The equations are as follows:

$$R = 1/(a + b \log_{10} W) \quad (5)$$

$$a = c + d L + e L^2 \quad (6)$$

$$b = f + g L + h L^2 \quad (7)$$

where R = cross-product statistic, W = weighting factor (coded), L = level of disintegration, a and b are functions of level of disintegration, and c through h are regression coefficients in the equations for a and b, quantified as follows for a 1,000-pixel (20 x 50) matrix:

$$c = 1.758037 \times 10^{-3}$$

$$d = -5.364542 \times 10^{-4}$$

$$e = 5.429313 \times 10^{-5}$$

$$f = 7.737475 \times 10^{-4}$$

$$g = -1.921002 \times 10^{-4}$$

$$h = 1.947964 \times 10^{-5}$$

The goodness-of-fit was 0.99 for the first equation, 0.94 for the second, and 0.95 for the third. Thus we have demonstrated that a general equation exists that will describe the general cross-product statistic of land-water patterns in simulated marshes as a function of weighting factor and level of disintegration. When equation (5) is solved for W, as follows:

$$W = \text{antilog}_{10} \{[1/(R\ b)] - a/b\} \quad (8)$$

we have an equation that, with the calculated coefficients, allows us to determine W (and G = W) for any R from a pixel of any size and configuration for which the coefficient c through h have been calculated. (The coefficients c through h given above apply only to a 1000-pixel matrix with a configuration of 2.5.)

Equipment limitations may prevent us from obtaining the R-mean values with which to calculate c through h coefficients for marshes the size of sample marshes from the imagery. It should, however, be possible to convert the R of an imagery marsh to that of a smaller-sized marsh. That R, along with c to h coefficients calculated from R-mean values of a marsh of the same size and configuration, could then be used to determine the best weighting factors for simulating the patterns of land and water in the imagery marsh. The effect of configuration makes it necessary for us to calculate, for the simulated marshes, R-mean values having the same configuration as the sample marshes of the imagery.

LSU ACTIVITIES

Two image processing facilities were utilized for this phase of the project, the Florida Department of Natural Resources Bureau of Marine Research in St. Petersburg and the Fisheries Image Processing System (FIPS) maintained by the NMFS in Slidell, Louisiana. Both facilities utilize the Earth Resources Laboratory Applications Software (ELAS) (Graham et al. 1984) developed by NASA to analyze remotely sensed digital data.

The TM data acquired for the project represented the only relatively cloud-free images available covering southeast Louisiana during the preferred period from November through February. The Landsat overflight occurred on 2 December 1984 (scene ID: 50276-16022), and the image encompasses most of the Mississippi Deltaic Plain.

Quads 1 and 2 of each of the seven TM bands were converted to an ELAS format and joined into a single data file using the ELAS modules TIPS and JTIPS (Graham et al. 1984).

The ELAS module STCI (Graham et al. 1984), a modified parallelepiped classifier, was used to generate an unsupervised classification on the basis of bands 2, 3, and 5. The STCI module creates a one-channel output file with 256 classes that closely resembles a three-channel color composite. We used the classified data to visually inspect the image for cloud cover and to facilitate selection of the first group of sample sites.

Clouds in the image were generally confined to upland areas and were not expected to interfere with the selection of sample sites in brackish- and salt-marsh areas. Selection of sample sites in fresh marshes, however, may be a problem because of the orientation of the abandoned delta lobes of the Mississippi River, limitations in the Landsat image's coverage of the area, and occasional cloud cover.

Selection of the Study Sites

The first study sites were selected in a salt marsh located on the Lafourche delta lobe, which was an actively prograding delta of the Mississippi River within the last 2,000 years. The study site corresponds to the area covered by five contiguous U.S. Geological Survey (USGS) 7.5-min. topographic quadrangles (Figure 16).

Historical trends in percentages of open water and shoreline lengths were tabulated for each of the five quadrangles from U.S. Fish and Wildlife Service (USFWS) habitat maps (Wicker et al. 1980). The maps are stored in a digital data base maintained by USFWS as a part of the Map Overlay and Statistical System (MOSS) (Lee 1984), a computerized spatial information system used for a number of applications in coastal management (Ader and Stayner 1982). The habitat maps are categorized according to the classification system of Cowardin et al. (1979) for estuarine and

deepwater habitats and are based on manual interpretations of aerial photographs taken in 1956 and 1978 (Wicker 1980).

An increase in the areal extent of water in the sample sites during 1956-78 was accompanied by a marked increase in shoreline length in three of the five quadrangles (Table 9). Shoreline lengths in the Central Isles Dernieres and Lake La Graisse decreased during the same period, reflecting the effects of erosional processes on coastal barriers and natural levee remnants adjacent to tributaries.

Evaluation of the Shoreline-Length Software

The ELAS module SLIN (Graham et al. 1984) is designed to measure the interface length between two adjacent land covers in digital thematic maps derived from remotely sensed data. The module was originally developed to measure shoreline lengths in Landsat images of coastal areas. The module utilizes the 3 x 3 moving-window technique and user-specified parameters to (1) detect shoreline pixels within the window, and (2) assign a numeric value to the center pixel on the basis of configuration of the shoreline within the window. Each interface pixel is assigned to one of 69 possible classes; two additional classes accommodate cases where all nine pixels in the mask are either land or water. Thus SLIN creates a new image file containing land, water, and shoreline pixels with class values ranging from 0 to 71. SLIN tabulates the shoreline length by associating the number of pixels in the 69 interface classes with 23 distance coefficients derived from multiples of diagonals and half-sides of a square pixel. Dow and Pearson (1982) identified at least three factors that can affect shoreline-length measurements made by

the SLIN module:

- o map scale
- o degree of reticulation in the shoreline
- o method used to segment the image into land and water.

Since this study will rely heavily on shoreline-length information derived from TM imagery, we devised an experiment to examine possible sources of errors in the SLIN module's measurements. USFWS digital habitat maps of the sample sites for the years 1956 and 1978 provided a convenient and reliable source of data for the experiment.

MOSS commands were used to create two types of polygon maps for the experiment, line maps consisting of shorelines only and maps with all of the habitat classes aggregated into land and water. The second stage of processing was undertaken in three steps. First, shoreline lengths were tabulated from the shoreline map using the length command in MOSS (Lee 1984). Second, the land-water polygon maps were converted to 30-m grid cells and reformatted for processing in ELAS. The final step consisted of tabulating the shoreline length for each cell map using the SLIN module. Thus, two measurements of shoreline length were available for each map: (1) the "true" shoreline length determined from the polygon map and (2) shoreline length derived from the 30-m-cell maps with the SLIN module.

A preliminary analysis of the relationship between shoreline lengths determined from the polygon maps and the 30-m-cell maps was conducted using linear regression analysis. For this initial analysis, the slope and intercept values of the line were estimated using ordinary least-squares (Upton and Fingleton 1985). The coefficient of simple determination (r^2) was 0.89. Although the sample size ($n = 10$) is relatively

small, the relationship seems to indicate that the 30-m-cell maps tend to underestimate the true shoreline length (Figure 17). A plot of the residuals revealed that the Dog Lake and Cocodrie quadrangles had more variability than the other three areas. Both quadrangles have highly reticulated shorelines and may be more difficult to measure accurately with the SLIN modules than are the other three areas.

Future work on the experiment will include the selection of a second group of study sites, which will provide additional observations for the model. The relationship between map scale and shoreline lengths will also be explored as a possible source of variation.

Image Processing for the Sample Sites

The ELAS modules PMGC and PMGE (Graham et al. 1984) were used to rotate the section of the band-5 image containing the sample sites to a Universal Transverse Mercator (UTM) north-south orientation for further processing. Rotation of the image was necessary because most ELAS modules require images to be projected in a UTM north-south orientation for proper functioning. A total of 65 ground control points (GCP) were selected from an interactive display of the band-5 image. UTM coordinates of corresponding points were determined from USGS 7.5-min topographic maps using an x-y digitizer. The image was rotated to a UTM north-south orientation by (1) computing a least-squares transformation equation from the GCP coordinates and (2) resampling the image using the technique of bilinear interpolation. Root-mean-square errors for the 65 points ranged from 8 to 208 m. with an average error of 52 m.

In spite of the great improvement in the ground resolution of TM data versus the older multispectral scanner data, very few fixed landmarks were available for use as GCPs. In the absence of fixed GCPs, the

alternative was to select relatively stable landmarks such as oil field and pipeline canal intersections. The accuracy of GCPs selected in Lake LaGraisse and the Central Isles Dernieres quadrangles, however, is highly questionable. The GCPs available in these areas were primarily located on the perimeters of coastal barriers and on shorelines around the remains of natural levee systems. Erosion and other coastal processes apparently altered the appearance of most landforms used for GCPs between the time of the 1984 TM overflight and the most recent (mid-to-late-1970's) USGS topographic maps available for the areas. As a result, GCPs selected in the Lake La Graisse and Central Isles Dernieres quadrangles generally had relatively high mapping errors, ranging from 100 to 200 m.

Two techniques for classifying the TM image into land and water were originally proposed for the project (1) gray-level thresholding of an image derived from ratioing the band-3 image, which represents the visible red portion of the spectrum, with one of the three infrared bands and (2) creating a land-water map from an unsupervised classification derived from a subset of the TM bands.

Band-ratioing seemed to have a high potential for producing an image with a sharp demarcation between the vegetated marsh surface and open-water areas. Periodic noise in the images, however, was a problem. Periodic noise in TM images has been described by other investigators (e.g., Wrigley et al. 1985, Bernstein et al. 1984) and was visually evident in open-water areas of bands 4, 5, and 7. Although the effect on individual bands seemed to be minimal, the problem worsened when the first ratioed image was generated from bands 3 and 5. This was expected, since noise is seldom correlated between bands, and image-enhancement techniques based on band ratios tend to enhance the uncorrelated content

of the two images (Moik 1980). Because techniques for removing periodic noise were not available at either image-processing facility, we rejected band ratios in favor of a simple technique based on gray-level thresholding of one of the three infrared bands.

Gray-level thresholding of remotely sensed infrared images is a relatively simple technique used to segment images of coastal areas into land and water. Determining the threshold between two classes, however, can be difficult in cases where the image is noisy or the valley between the bimodal peaks in the gray-level histogram is relatively wide. Techniques for selecting thresholds can be divided into two groups: (1) interactive selection of a threshold based on a priori knowledge of the area of interest and (2) empirical methods for improving the image histogram to facilitate the selection of a threshold (e.g., Kirby and Rosenfield 1979; Pun 1981; Weszka and Rosenfield 1978).

Shoreline-length measurements taken from land-water images derived from thresholded TM data can vary greatly depending upon where the threshold is selected in the image histogram. This effect is illustrated in Figure 18, which shows the relationship between threshold selection and shoreline-length measurements taken with the SLIN module from the band-5 image of the study sites. When water pixels were defined as having a value of 5, the lowest threshold tested, or less, noisy pixels in the open-water areas were classified as land and tended to increase shoreline lengths. Shoreline length was minimal at a gray level of 7 but increased steadily as the threshold moved upward to a value of 25; between digital-count 25 and 50, shoreline lengths abruptly declined. The actual threshold between land and water appears to fall in the range between digital-count values 7 and 15 in the band-5 image.

We are continuing to evaluate the utility of various image-processing techniques for segmenting the TM data into land-water images.

FUTURE ACTIVITIES

Our first activity in Miami during the third semiannual period will be conversion of the model to the language C for implementation on our AT&T Unix PC microcomputer. When this is accomplished, we will explore the practical upper limits to the size of a marsh-matrix that can be simulated, considering that we have to make numerous simulations with different weighting factors and that each must have 30 replications.

At a meeting in Baton Rouge on May 30, we decided that sample marshes from the imagery should be the size of one-quarter quadrangle. A quadrangle is approximately 475 rows by 425 columns (in terms of pixels), after the sides have been smoothed. The following table shows how a matrix of approximately that size can be reduced to one-quarter size in consecutive steps by dividing rows and columns by two each time.

Marsh Matrix	Rows	Columns	Number of Pixels	Row/Col. Ratio Configuration
1	464	416	193,024	1.1154
2	232	208	48,256	1.1154
3	116	104	12,064	1.1154
4	58	52	3,016	1.1154
5	29	26	754	1.1154

We will attempt to simulate marshes the size of (2) above, which is approximately the same size as the sample marshes of the imagery. If that is not possible, we will try to simulate marshes of size (3) or (4)

above. If that size is impractical, we already know that we can simulate marshes of size (5).

If we are not able to simulate a marsh as large as that of the sample marsh from the imagery, then we will translate the R measured on the imagery to the equivalent R for a smaller marsh of the same configuration, using the following equation.

$$R_{m4} = (R_{m2}\ E(R)_{m4})/E(R)_{m2} \qquad (9)$$

where R_{m2} = cross-product statistic of the sample marsh from the imagery, R_{m4} = cross-product statistic of the smaller marsh $E(R)_{m2}$ = expected value of the cross-product statistic of the sample marsh from the imagery, and $E(R)_{m4}$ = expected value of R of the smaller marsh. Preliminary calculations suggest that the error involved in a conversion of this type is small, provided the matrices have the same configuration.

Having determined which matrix is both practical to simulate on our computer system and of the same configuration as that of sample marshes from the imagery, we will run 30-replicate simulations to obtain R-means for various weighting factors and levels of disintegration. The c through h coefficients for our three equations for a family of curves will be calculated from these R-means. Following the calculation of these coefficients, we will determine the accuracy of the equations by comparing Rs calculated from the equations to the R-means (from the simulations) used to calculation the c through h coefficients.

If the simulated marshes are not the same size as the sample marshes from the imagery, it will be necessary to evaluate the accuracy of our method of converting an R value for a matrix one size to an equivalent R value of a smaller matrix. We will do this by simulating marshes of a

still smaller size than our selected simulation size and determining R-means for the various weighting factors and levels. We will then calculate, from the R for the larger marsh size, an equivalent R for the smaller marsh size, which can then be checked against the R-mean from the simulations.

Activities at LSU for the next semiannual period will center on incorporating additional software into ELAS, testing the accuracy of the software, comparing results from ELAS measurement methods to results of measurement methods used on the simulated marshes, selecting and preparing new quadrangles of imagery to include in the analysis, and performing spatial-pattern parameter analysis on the imagery already selected. Having set the size of sample marshes at one quarter of a quadrangle. We will divide each selected quadrangle into quarters and analyze each quarter.

Early in the new semiannual period, we will select additional salt-marsh quadrangles from a delta lobe having geological history different from that of the Lafourche lobe, which is represented by the five quadrangles already selected. Then we will georeference the new areas and begin analyzing the 1956 and 1978 USFWS habitat maps for these areas. The habitat-map data will be used to provide additional data points for continued testing of the accuracy of SLIN for measuring shoreline length.

Software modules for estimating spatial pattern parameters for sample marshes from TM imagery have been prepared and are presently stored on tape in Slidell, but have not yet been incorporated into ELAS. This task will be given high priority in the coming semiannual period.

Following implementation of these modules, ELAS will be used to collect the following data on the first 20 sample marshes:

1. water area as percentage of the total area,
2. length of the land-water interface
3. maximum possible interface
4. cross-product statistic (R)

Later, the following additional statistics will have to be collected on the same samples:

5. frequency distribution of pixels in terms of number of sides adjacent to other water pixels
6. percent total pixels on each row from main water body that are water pixels
7. frequency distribution of water bodies by size (number of pixels)
8. frequency distribution of pixels by water-body size

The expected value of the cross-product statistic, E(R), for a marsh the same size as the sample marsh will be calculated independently in Miami. Although a module for the calculation of E(R) has been included as one of the modules mentioned above, it is so time-consuming to execute that it may not be practical to use it in the ELAS framework.

Once measurements 1-4 above have been completed for some sample marshes, they will be sent to Miami so that the correct weighting factors can be selected to simulate marshes with similar spatial patterns. The patterns simulated will then be checked for similarity to the sample marshes of the imagery by comparing parameters 5-8.

The SLIN module of ELAS measures interface length differently from the way it is measured on the simulated marshes. Since in both cases

interface length is expressed as a percentage of maximum possible interface length, the different measurement methods may not cause a problem. However, we need to ensure that the difference in measurement method does not introduce errors into our comparisons of TM marsh images and simulated marshes or that, if it does, we can correct for it. Therefore, we plan to use SLIN to measure interface and maximum possible interface on several simulated marshes for which we have also measured the two parameters by the more direct method employed on the simulations. Comparing SLIN-generated values to the other values should allow us to quantify the difference caused by measurement method, if any is present.

To apply the results of our study to natural resource problems, we need to know how the scale of our measurement unit has affected our measurements of shoreline length. During the next semiannual period, we plan to examine the effect of scale on our data.

ACKNOWLEDGMENTS

We wish to thank the following persons and organizations for their help on various aspects of the project: Ken Haddad, Florida Department of Natural Resources, Bureau of Marine Research; Andrew Kemmerer and Gerald Williamson, Mississippi Laboratories, National Marine Fisheries Service; and Larry Handley, Jim Scurry, and Floyd Stayner, National Coastal Ecosystems Team, U.S. Fish and Wildlife Service.

REFERENCES

Ader, R. R., and F. Stayner. 1982. The role of the USFWS geographic information system in coastal decision-making. Proceedings, Auto-Carto 5. ACSM-ASP, pp. 1-12.

Beaver, R., and W. Mendenhall. 1971. Introduction to Probability and Statistics, 3rd Edition. Belmont, Calif.: Wadsworth. 498 pp.

Bernstein, R., J. B. Lotspiech, J. H. Meyers, H. G. Kolsky, and R. D. Lees. 1984. Analysis and processing of Landsat-4 sensor data using advanced image-processing techniques and technologies. IEEE Transactions on Geoscience and Remote Sensing, Vol. GE-22, pp. 192-221.

Browder, J. A., H. A. Bartley, and K. S. Davis. 1985a. A probabilistic model of the relationship between marshland-water interface and marsh disintegration. Ecological Modelling 29:245-260.

Browder, J. A., L. N. May, Jr., A. Rosenthal, R. H. Baumann, and J. G. Gosselink. 1985b. First semi-annual progress report to NASA on the TM project: Utilizing remote-sensing of thematic mapper data to improve our understanding of estuarine processes and their influence on the productivity of estuarine-dependent fisheries. National Marine Fisheries Service, Miami, Fla., and Louisiana State University, Baton Rouge, La.

Cliff, A. D., and J. K. Ord. 1981. Spatial Processes: Models and Applications. London: Pion. 261 pp.

Cowardin, L. M., V. Carter, F. C. Golet, and E. T. LaRoe. 1979. Classification of wetlands and deepwater habitats of the United States. U.S. Fish and Wildlife Service, Office of Biological Services, Report No. FWS/OBS-79/31, 103 pp.

Dow, D. D. and R. W. Pearson. 1982. SLIN: a software program to measure interface length. NASA Earth Resources Laboratory, NSTL, Miss. Report No. 208. 19 pp.

Fishman, G. S. 1973. Concept and methods in discrete-event digital simulation. New York: Wiley. 386 pp.

Graham, M. H., B. G. Junkin, M. T. Kalcic, R. W. Pearson, and B. R. Seyfarth. 1984. ELAS: Earth Resources Laboratory applications software, Vol. II, ELAS user's guide. NASA Earth Resources Laboratory, NSTL, Miss. 428 pp.

Kirby, R. L., and A. Rosenfeld. 1979. A note on the use of (gray level, local average gray level) space as an aid in threshold selection. IEEE Transactions on Systems, Man, and Cybernetics, Vol. SMC-9, No. 12, pp. 860-864.

Lee, J. E. (ed.). 1984. MOSS User's Manual. U.S. Fish and Wildlife Service, Western Energy and Land Use Team, Ft. Collins, Colo. 443 pp.

Moik, J. G. 1980. Digital processing of remotely sensed images. National Aeronautics and Space Administration Scientific and Technical Information Branch, NASA SP-431. 330 pp.

Pun, T. 1981. Entropic thresholding, a new approach. Computer Graphics and Image Processing 16:210-239.

Upton, G., and B. Fingleton. 1985. Spatial Data Analysis by Example. Vol. 1. New York: Wiley. 410 pp.

Weszka, J. S., and A. Rosenfeld. 1978. Threshold evaluation techniques. IEEE Transactions on Systems, Man, and Cybernetics, Vol. SMC-8, No. 8, pp. 622-629.

Wicker, K. M. 1980. Mississippi Deltaic Plain Region ecological characterization: a habitat mapping study. A user's guide to the habitat maps. U.S. Fish and Wildlife Service, Office of Biological Services. FWS/OBS-79/07. 45 pp.

Wicker, K. M., J. B. Johnston, M. W. Young, and R. M. Rogers. 1980. The Mississippi Deltaic Plain Region habitat mapping study. 464 maps. U.S. Fish and Wildlife Service, Office of Biological Services. FWS/OBS-79/07.

Wrigley, R. C., C. A. Hlavka, and D. H. Card. 1985. Evaluation of thematic mapper interband registration and noise characteristics. Photogrammetric Engineering and Remote Sensing 51:1417-1425.

Table 1. Results of a chi-square test of the randomness of a mixed congruential random number generator on the Burroughs 6800.

Execution	Chi-square
1	4,085.88
2	4,137.37
3	4,105.87
4	4,121.87
5	4,095.37
6	3,956.01
7	4,157.24
8	4,048.13
9	4,148.00
10	4,051.25

Max Q' = 1.54 < 1.96, therefore do not reject H_0 at alpha = 0.05.

Table 2. Runs-up-and-down test for a mixed congruential random number generator on the Burroughs 6800 computer.

Execution	Runs-up-and-down
1	16*
2	21*
3	18*
4	23*
5	22*
6	19*
7	19*
8	22*
9	18*
10	20*

*Conclude H_0 -- the process is random at alpha = 0.1.

Table 3 E(R) as a function of level and matrix size

Matrix Size (20xN)	Level								
	.1	.2	.3	.4	.5	.6	.7	.8	.9
100	63.64	113.13	148.48	169.70	176.77	169.70	148.48	113.13	63.64
200	133.87	237.99	312.36	356.98	371.86	356.98	312.36	237.99	133.87
400	274.29	487.62	640.00	731.43	761.90	731.43	640.00	487.62	274.29
600	414.69	737.23	967.61	1105.84	1151.92	1105.84	967.61	737.23	414.69
800	555.09	986.83	1295.22	1480.25	1541.93	1480.25	1295.22	986.83	555.09
1000	695.50	1236.44	1622.82	1854.65	1931.98	1854.65	1622.82	1236.44	695.50

Table 4 VAR(R) as a function of level and matrix size

Matrix Size (20xN)	Level								
	.1	.2	.3	.4	.5	.6	.7	.8	.9
100	28.65	76.79	125.03	159.51	171.93	159.51	125.03	76.79	28.65
200	57.60	160.23	264.52	339.49	366.54	339.49	264.52	160.23	57.60
400	113.07	324.85	542.47	699.58	756.37	699.58	542.47	324.85	113.07
600	168.01	488.98	820.18	1059.68	1146.31	1059.68	820.18	488.98	168.01
800	222.83	652.99	1097.81	1419.79	1536.28	1419.79	1097.81	652.99	222.83
1000	277.60	816.95	1375.48	1779.91	1926.27	1779.91	1375.48	816.95	277.60

Table 5 E(R) as a function of level and R-mean as a function of level and weighting factors for Matrix size = 1000 (20 rows, 50 columns)

E(R)

Level

.1	.2	.3	.4	.5	.6	.7	.8	.9
695.50	1236.44	1622.82	1854.65	1931.93	1854.65	1622.82	1236.44	695.50

R-mean

Level

Weights W,G	.1	.2	.3	.4	.5	.6	.7	.8	.9
0,0	700.60	1243.60	1619.80	1873.50	1948.80	1865.40	1622.93	1236.46	694.53
4,4	554.93	918.00	1144.93	1274.60	1298.10	1254.73	1101.53	856.60	515.13
8,8	503.66	808.80	1006.73	1097.80	1145.70	1104.60	988.46	767.53	475.46
12,12	469.00	746.20	908.00	1028.53	1048.70	1028.40	900.13	721.73	449.00
24,24	401.73	638.93	774.47	879.53	896.60	856.00	766.66	620.30	382.86
76,76	302.06	473.93	590.53	635.86	654.06	642.86	580.33	455.33	291.46

Table 6 VAR(R) as a function of level and sample variance as a function of level and weighting factors for Matrix size = 1000 (20 rows, 50 columns)

VAR(R)

Level

.1	.2	.3	.4	.5	.6	.7	.8	.9
277.60	816.95	1375.48	1779.91	1926.27	1779.91	1375.48	816.95	277.60

Sample variance

Level

Weights W,G	.1	.2	.3	.4	.5	.6	.7	.8	.9
0,0	232.54	883.97	1493.76	1114.18	1347.07	2203.13	1996.84	602.71	221.87
4,4	396.78	1223.73	1759.21	3010.93	2560.85	2790.99	2286.98	2011.81	1013.51
8,8	425.48	1124.04	2754.44	2313.39	3985.49	2748.25	4479.07	2238.34	1094.57
12,12	456.87	1851.10	2060.61	2884.95	3773.62	3990.46	4108.07	3071.65	1444.02
24,24	652.46	1517.41	3814.80	3541.75	3385.53	3678.80	4488.29	2788.60	2236.48
76,76	684.48	2410.87	3594.60	3073.83	6561.84	5353.72	5423.00	5127.40	2938.00

Table 7. Expected value, E(R), and variance, var(R), of the cross-product statistic for paired matrices of the same size (number of pixels) but different configurations (ratios of rows to columns). (The ratio or its inverse is given in parentheses above each value.) All matrices are disintegrated to the 0.5 level.

Matrix Size	N	E(R) Rows and Columns 20 X N		10 X 2N	
100	5	176.77	(4)	181.82	(1)
200	10	371.86	(2)	371.86	(2)
400	20	761.90	(1)	751.88	(4)
600	30	1,151.92	(1.5)	1,131.89	(6)
800	40	1,541.93	(2)	1,511.89	(8)
1,000	50	1,931.93	(2.5)	1,891.89	(10)

Matrix Size	N	var(R) Rows and Columns 20 X N		10 X 2N	
100	5	171.93	(4)	176.68	(1)
200	10	366.54	(2)	366.54	(2)
400	20	756.37	(1)	746.48	(4)
600	30	1,146.31	(1.5)	1,126.46	(6)
800	40	1,536.28	(2)	1,506.45	(8)
1,000	50	1,926.27	(2.5)	1,886.44	(10)

Table 8. Expected value, E(R), and variance, var(r), of the cross-product statistic for matrices of (a) different sizes but the same configuration (ratio of rows to columns or the inverse) and (b) the same size but different configurations. All matrices are disintegrated to the 0.5 level.

(a) E(R) and var(R) for matrices with a configuration of 1.0.

Rows and Columns	Matrix Size	E(R)	var(R)
10 X 10	100	181.82	176.68
15 X 15	225	421.87	416.46
20 X 20	400	761.90	756.37
25 X 25	625	1,201.92	1,196.29
30 X 30	900	1,741.94	1,736.25

(b) Paired matrices of the same size but different configurations (Configuration given in parentheses.)

Rows X Columns	Matrix Size	E(R)		var(R)
5 X 200	1,000	1,796.80	(40)	1,791.88
10 X 100	1,000	1,891.89	(10)	1,886.44
20 X 50	1,000	1,931.93	(2.5)	1,926.27
25 X 40	1,000	1,936.94	(1.6)	1,931.25

Table 9. Changes in water area and shoreline length tabulated from USFWS habitat maps for each of the five quadrangles comprising the study area, 1956-78.

Quadrangle name	Water[a]			Shoreline		
	Percentage of total area		1956-78	Length (km)		1956-78
	1956	1978	change (%)	1956	1978	change (%)
Grand Bayou Du Large	61.8	67.4	9.1	542.4	730.0	34.6
Dog Lake	39.1	51.8	32.4	879.0	1,408.5	60.2
Cocodrie	51.6	62.8	21.7	540.1	960.2	77.8
Lake La Graisse	93.9	96.8	3.1	154.0	132.3	-14.1
Central Isles Dernieres	76.8	89.5	16.5	383.1	337.9	-11.8
Totals	64.7	73.7	13.9	2,498.6	3,568.9	42.8

[a]Includes USFWS habitat categories: E1OWH (open water), E1OW (leveed and impounded water bodies), E1O1WO (oil and gas canals), E1OWX (excavated open water), E1AB (aquatic beds), and E3FL (sand, shell, and mud flats).

LIST OF FIGURES

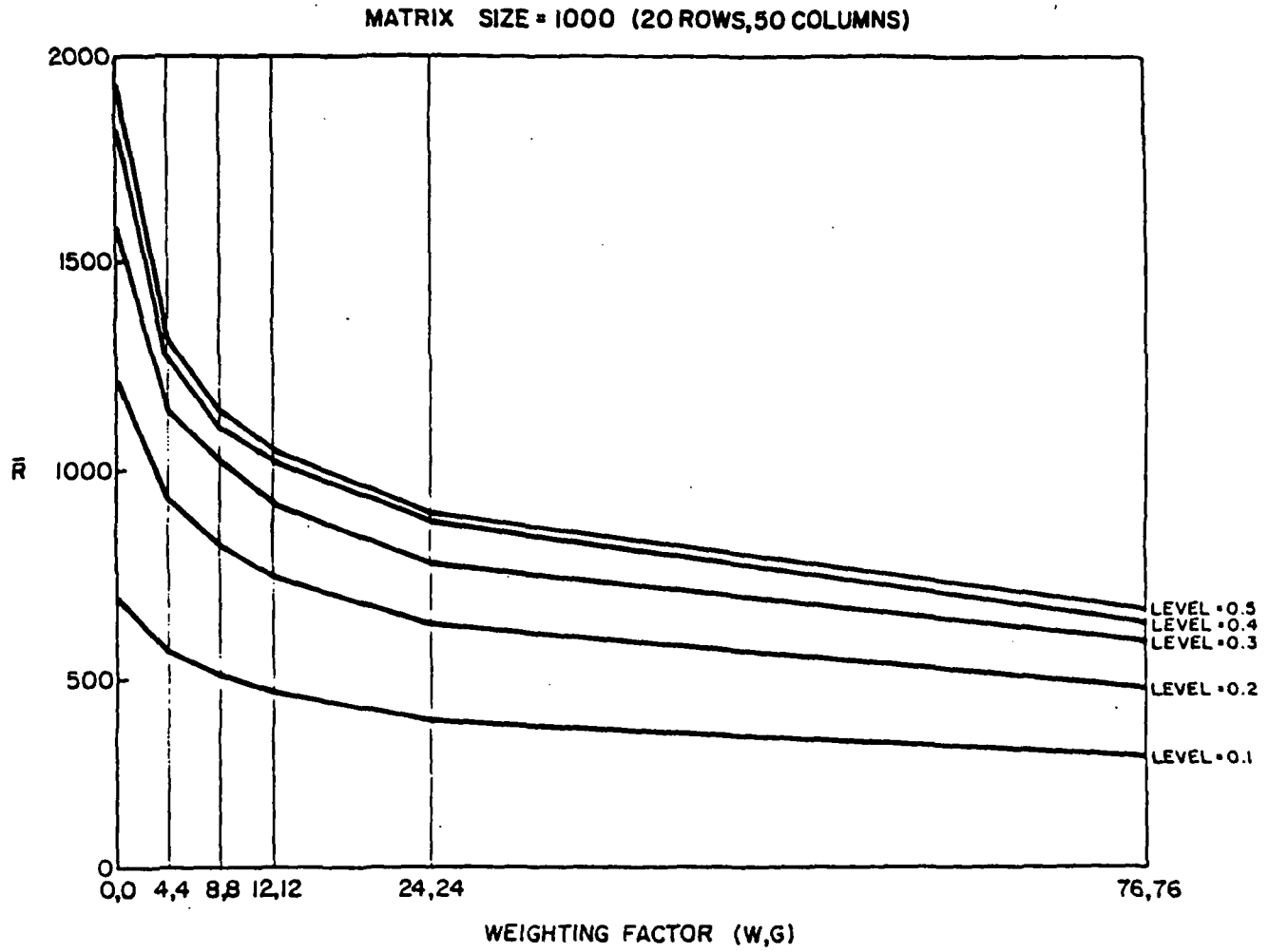

Figure 1. Plot of R-mean vs. weighting factors W and G = W for a 1,000-pixel matrix at five levels of disintegration.

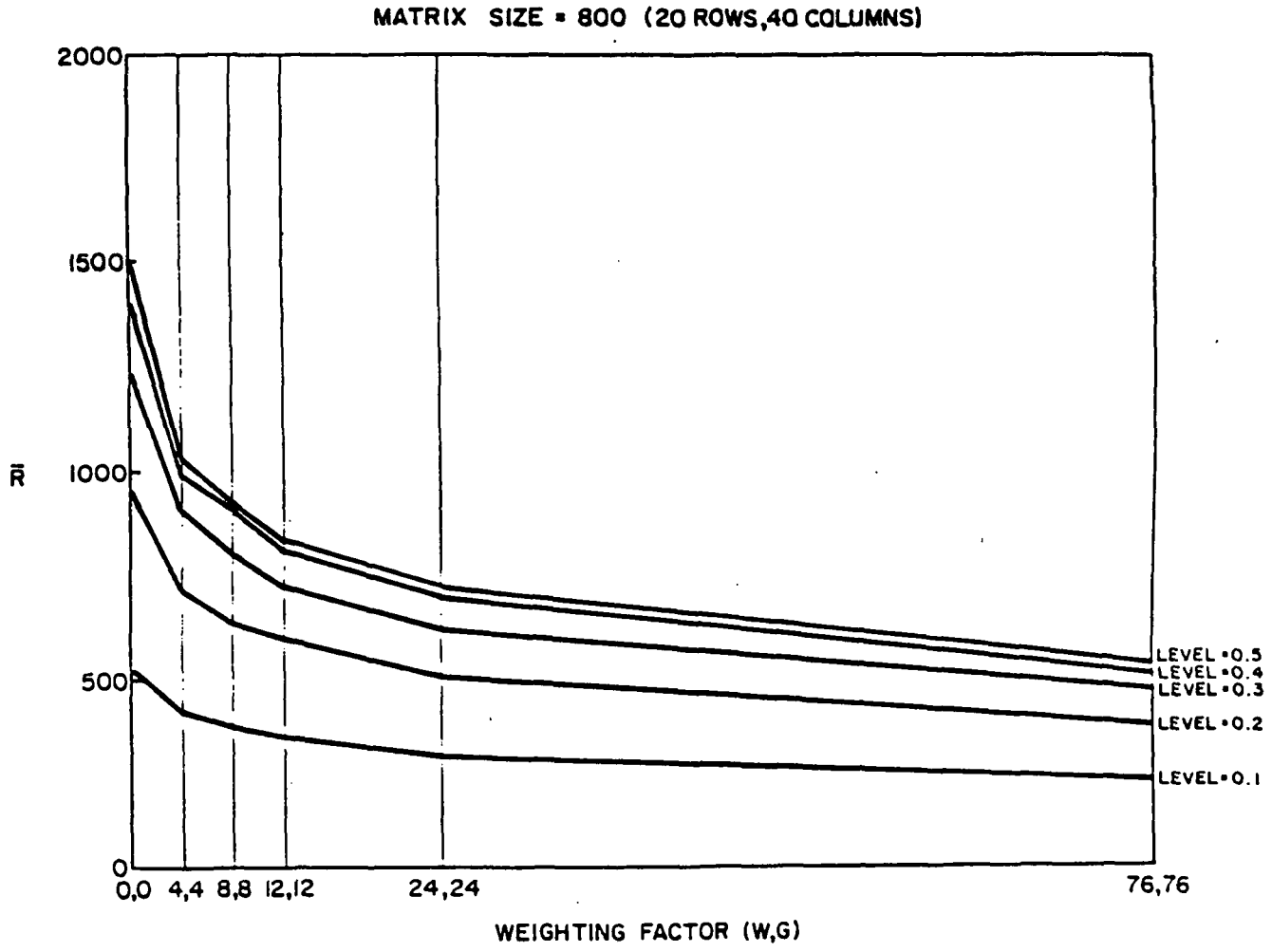

Figure 2. Plot of R-mean vs. weighting factors W and G = W for an 800-pixel matrix at five levels of disintegration.

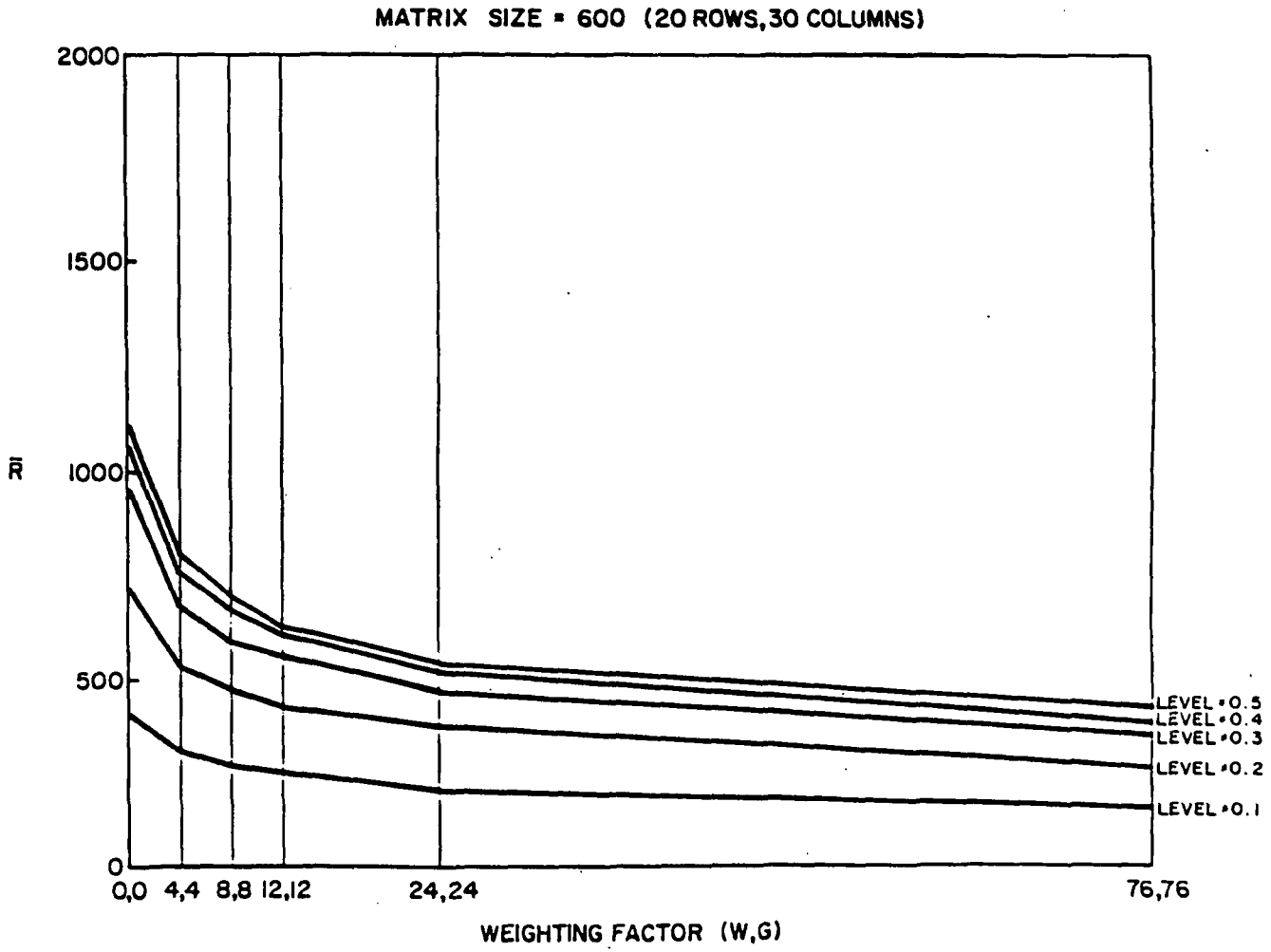

Figure 3. Plot of R-mean vs. weighting factors W and G = W for a 600-pixel matrix at five levels of disintegration.

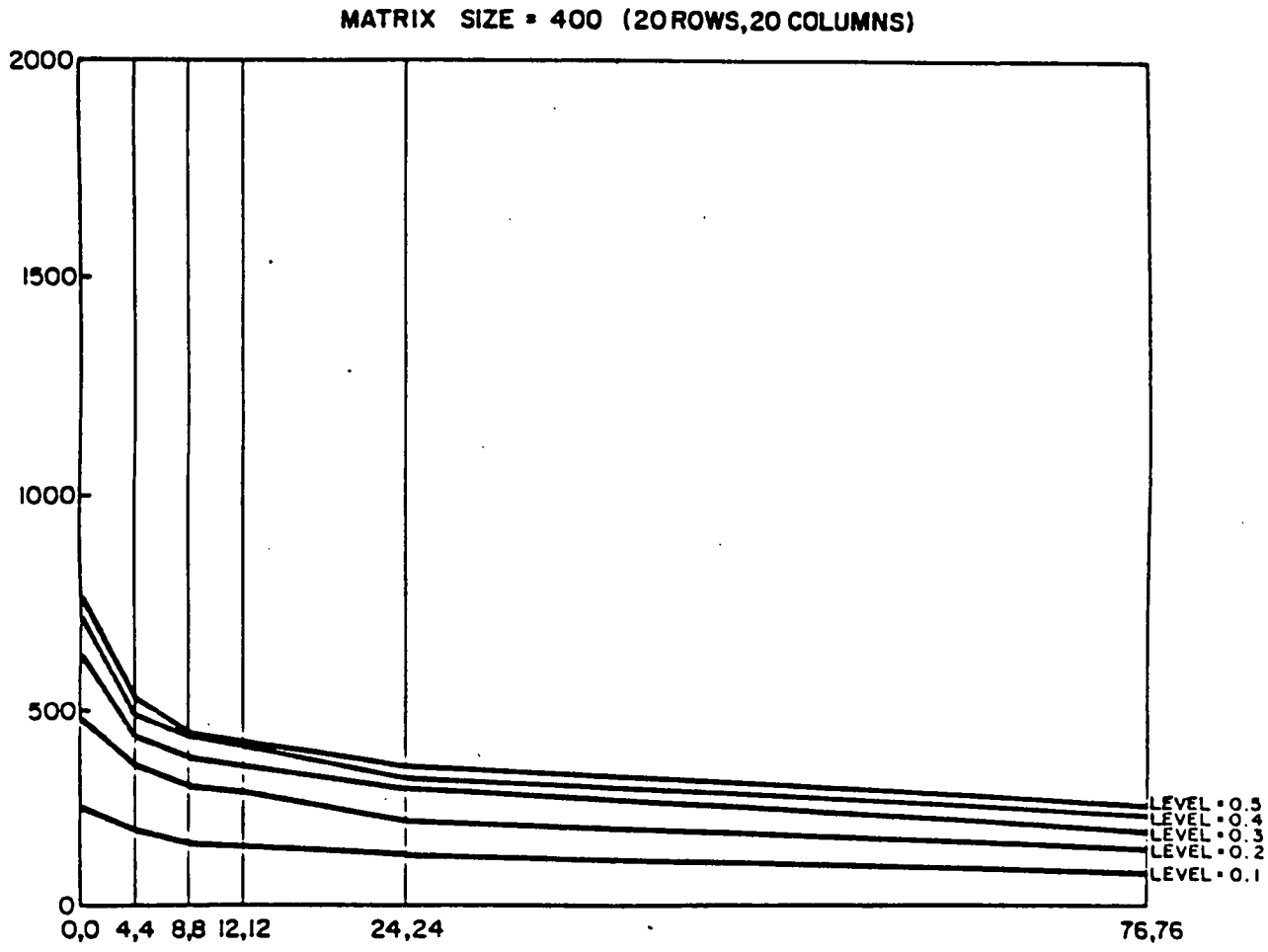

Figure 4. Plot of R-mean vs. weighting factors W and G = W for a 400-pixel matrix at five levels of disintegration.

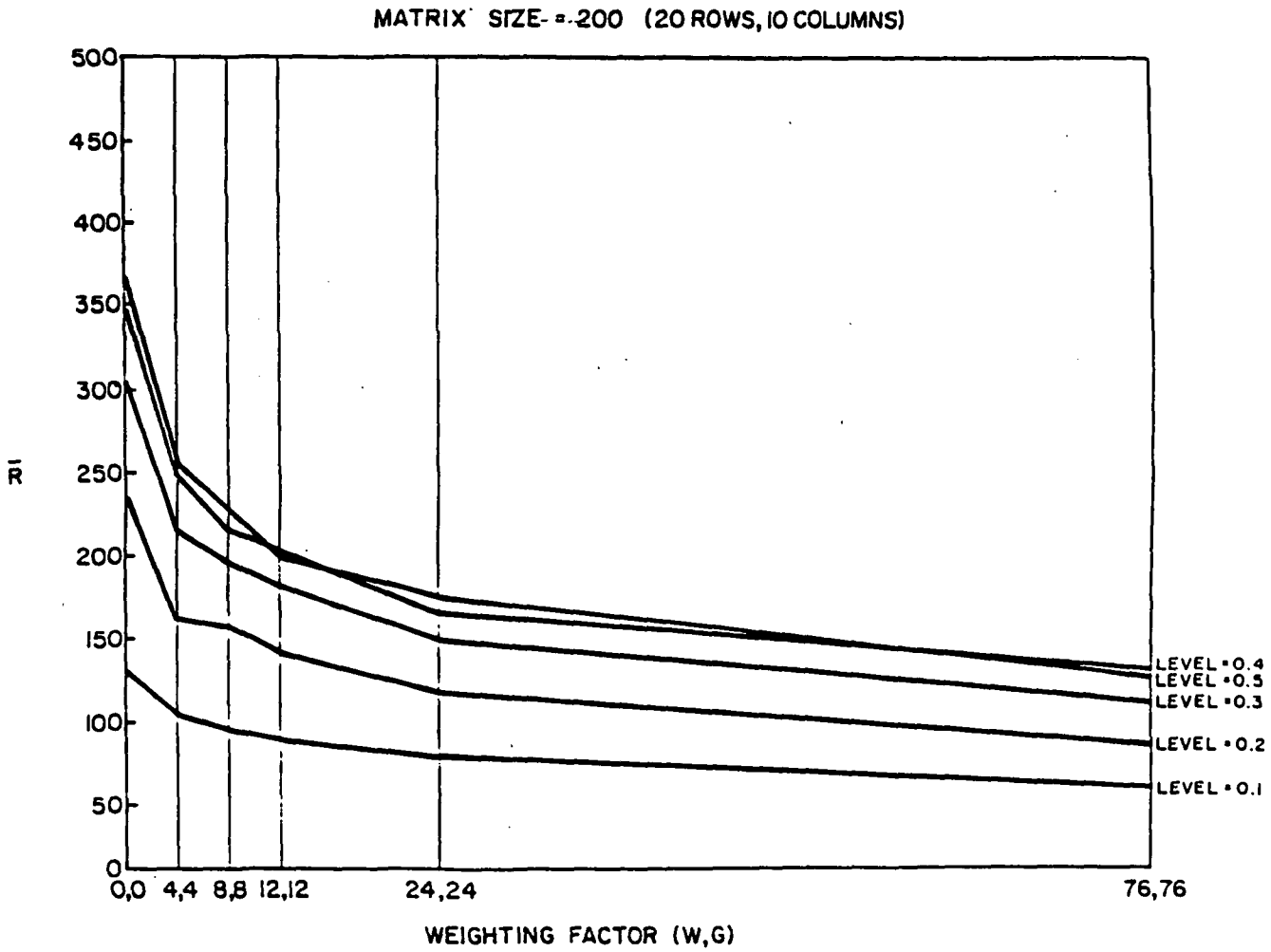

Figure 5. Plot of R-mean vs. weighting factors W and G = W for a 200-pixel matrix at five levels of disintegration.

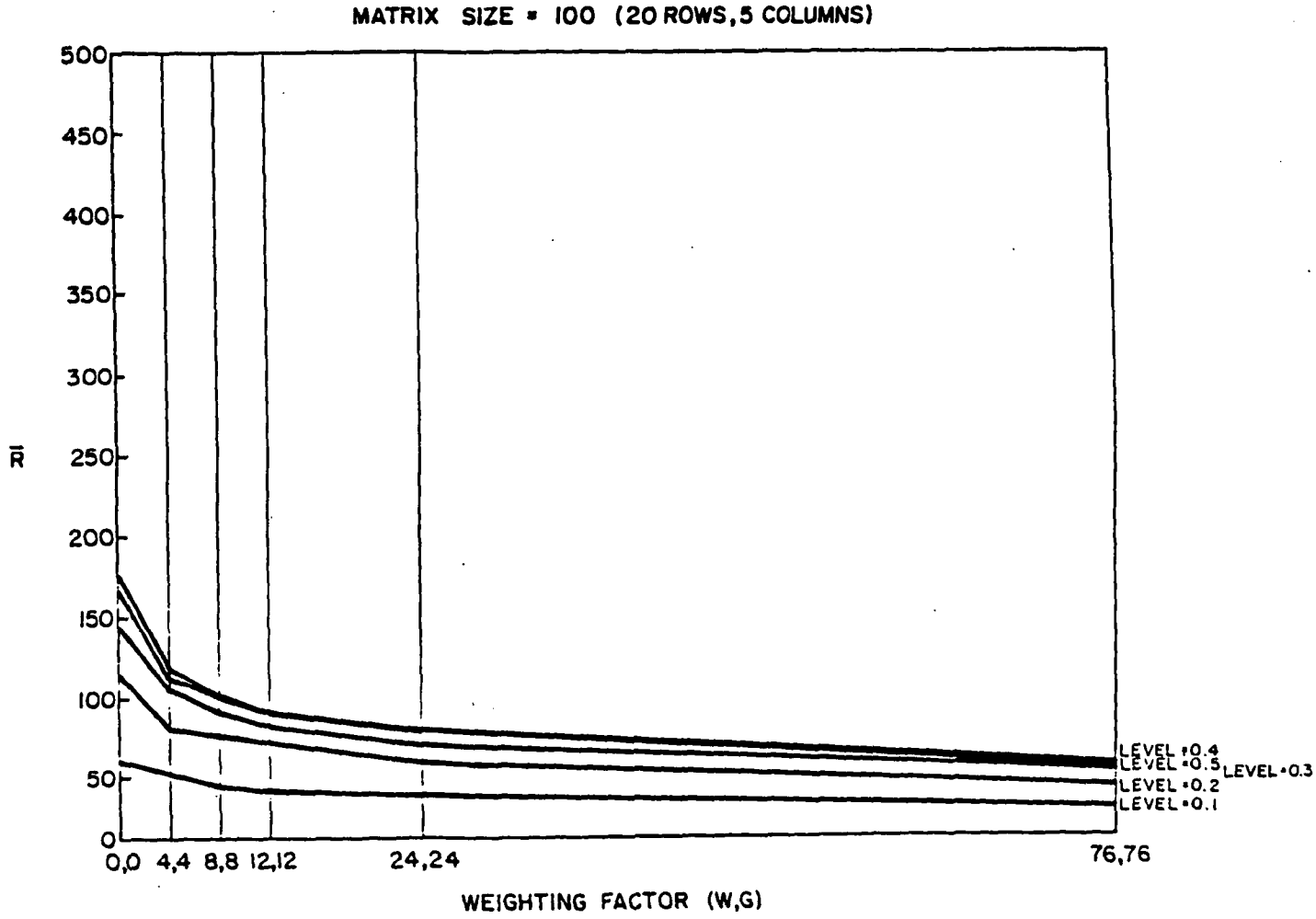

Figure 6. Plot of R-mean vs. weighting factors W and G = W for a 100-pixel matrix at five levels of disintegration.

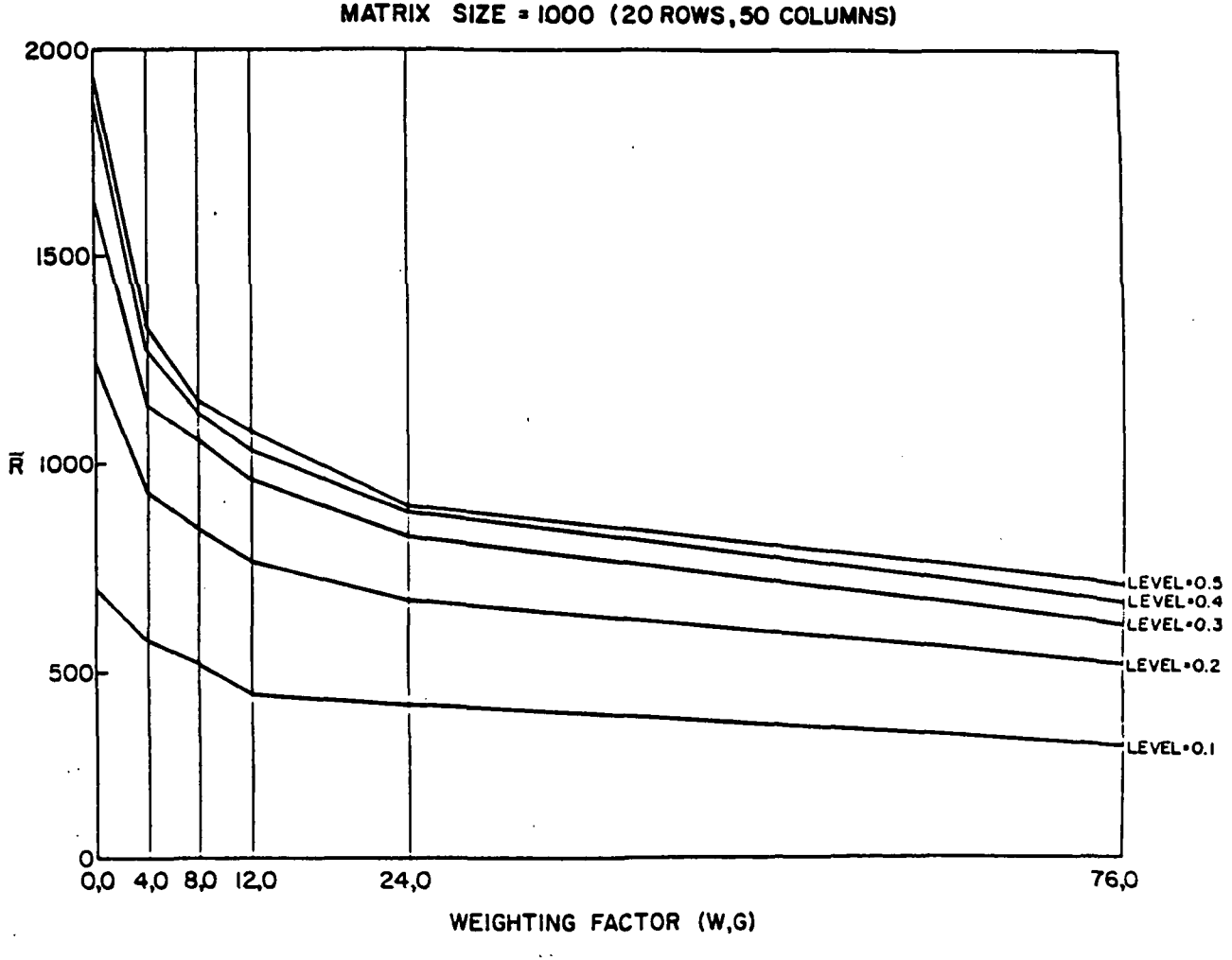

Figure 7. Plot of R-mean vs. weighting factors W and G = 0 for a 1,000-pixel matrix at five levels of disintegration.

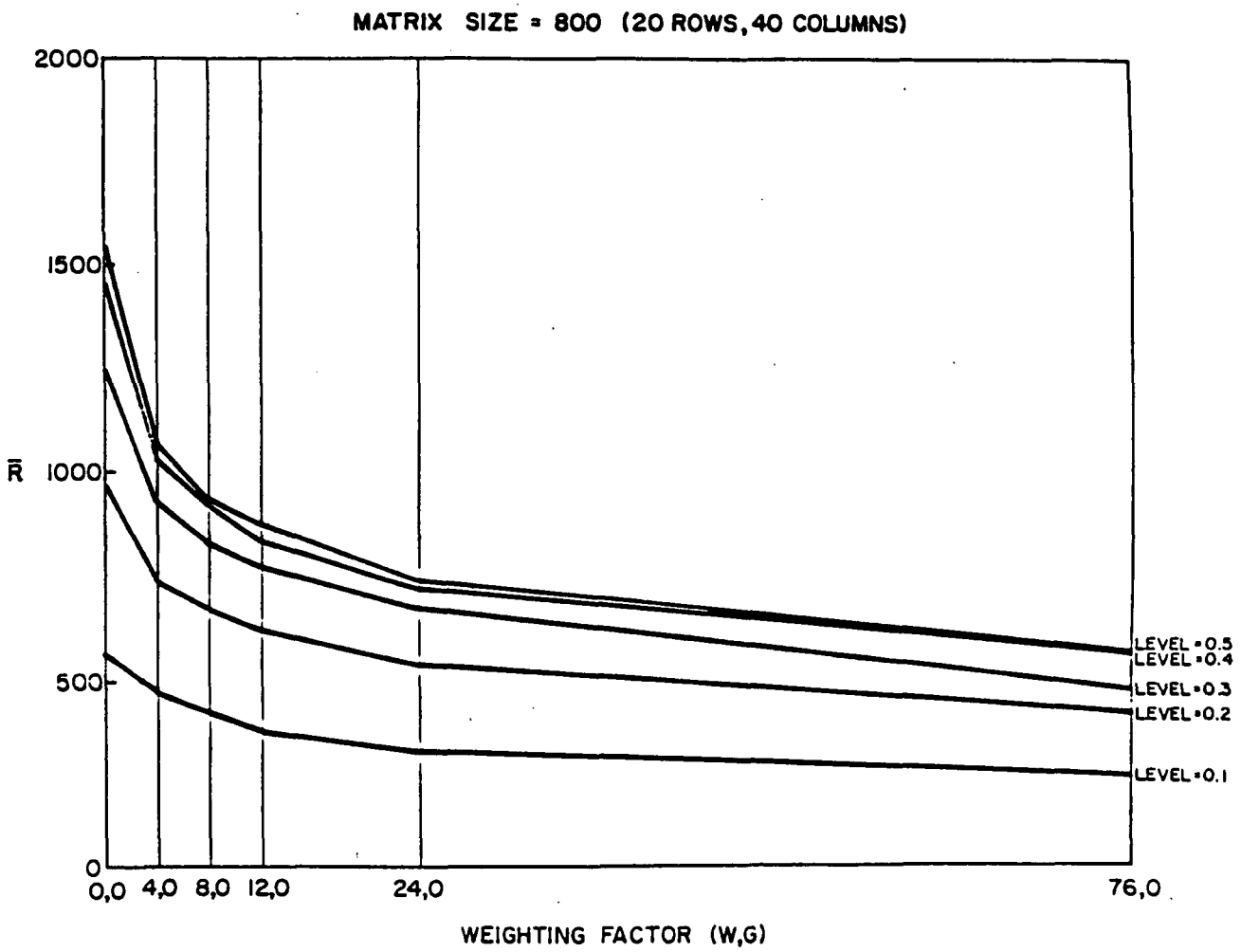

Figure 8. Plot of R-mean vs. weighting factors W and G = 0 for an 800-pixel matrix at five levels of disintegration.

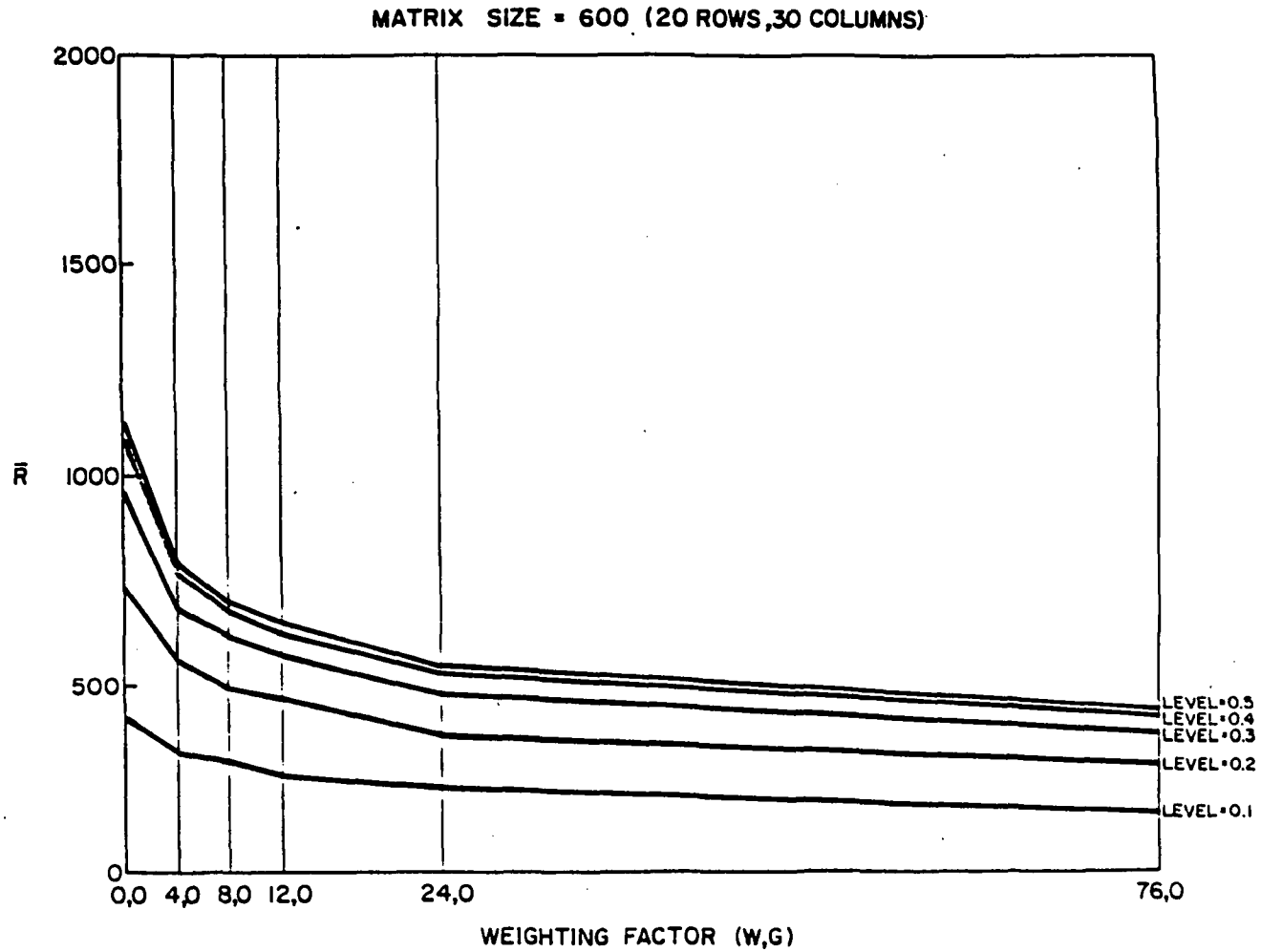

Figure 9. Plot of R-mean vs. weighting factors W and G = 0 for a 600-pixel matrix at five levels of disintegration.

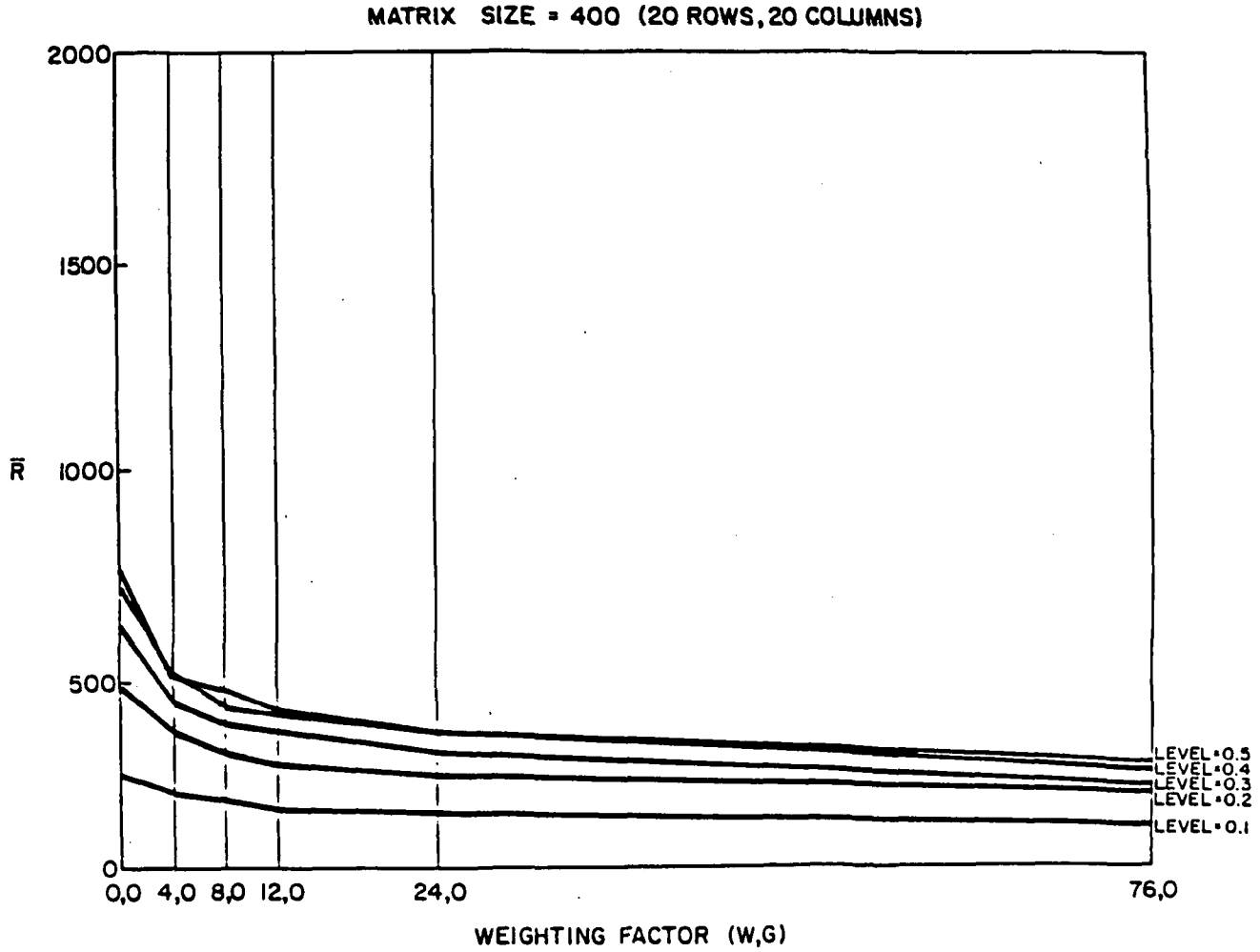

Figure 10. Plot of R-mean vs. weighting factors W and G = 0 for a 400-pixel matrix at five levels of disintegration.

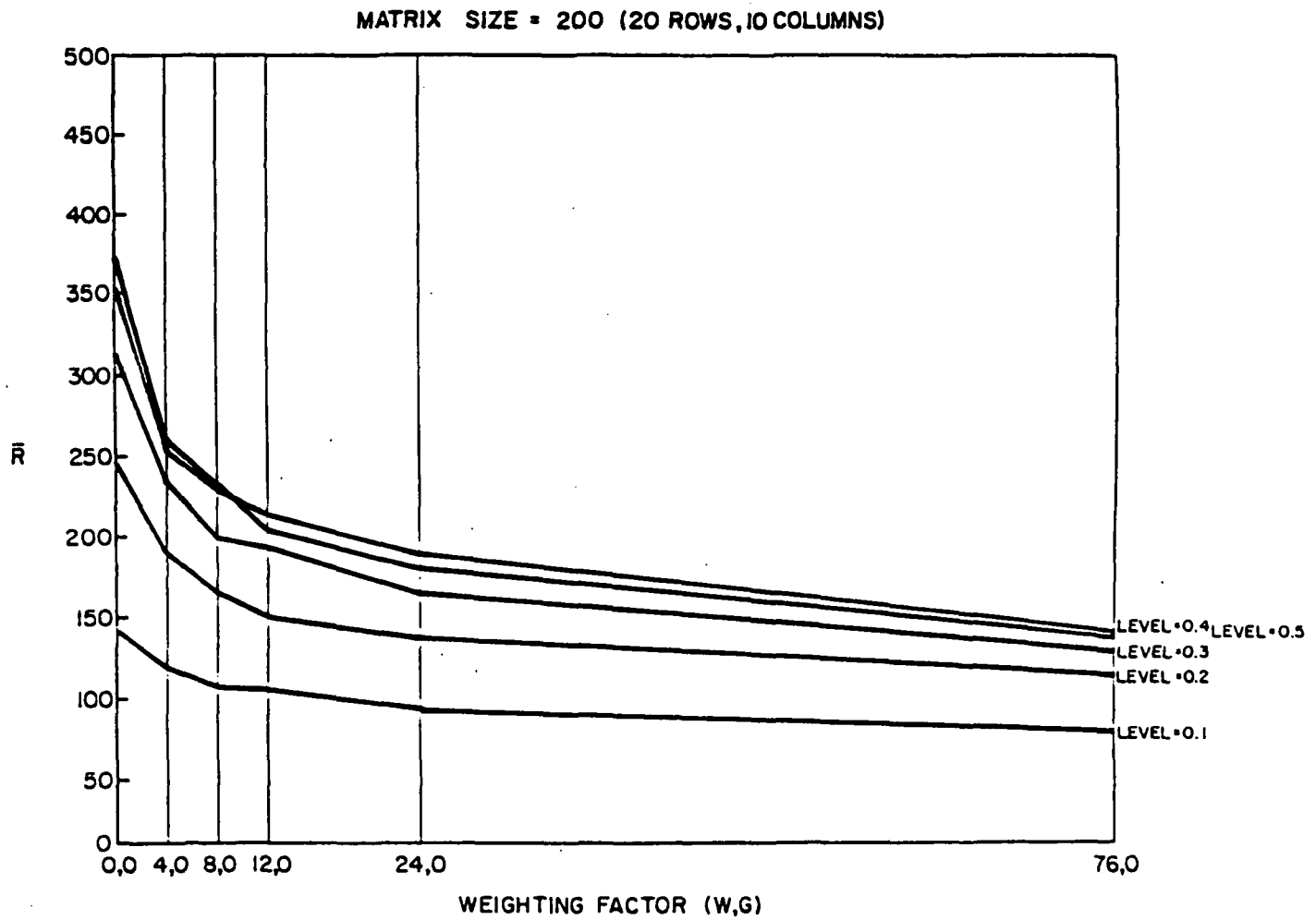

Figure 11. Plot of R-mean vs. weighting factors W and G = 0 for a 200-pixel matrix at five levels of disintegration.

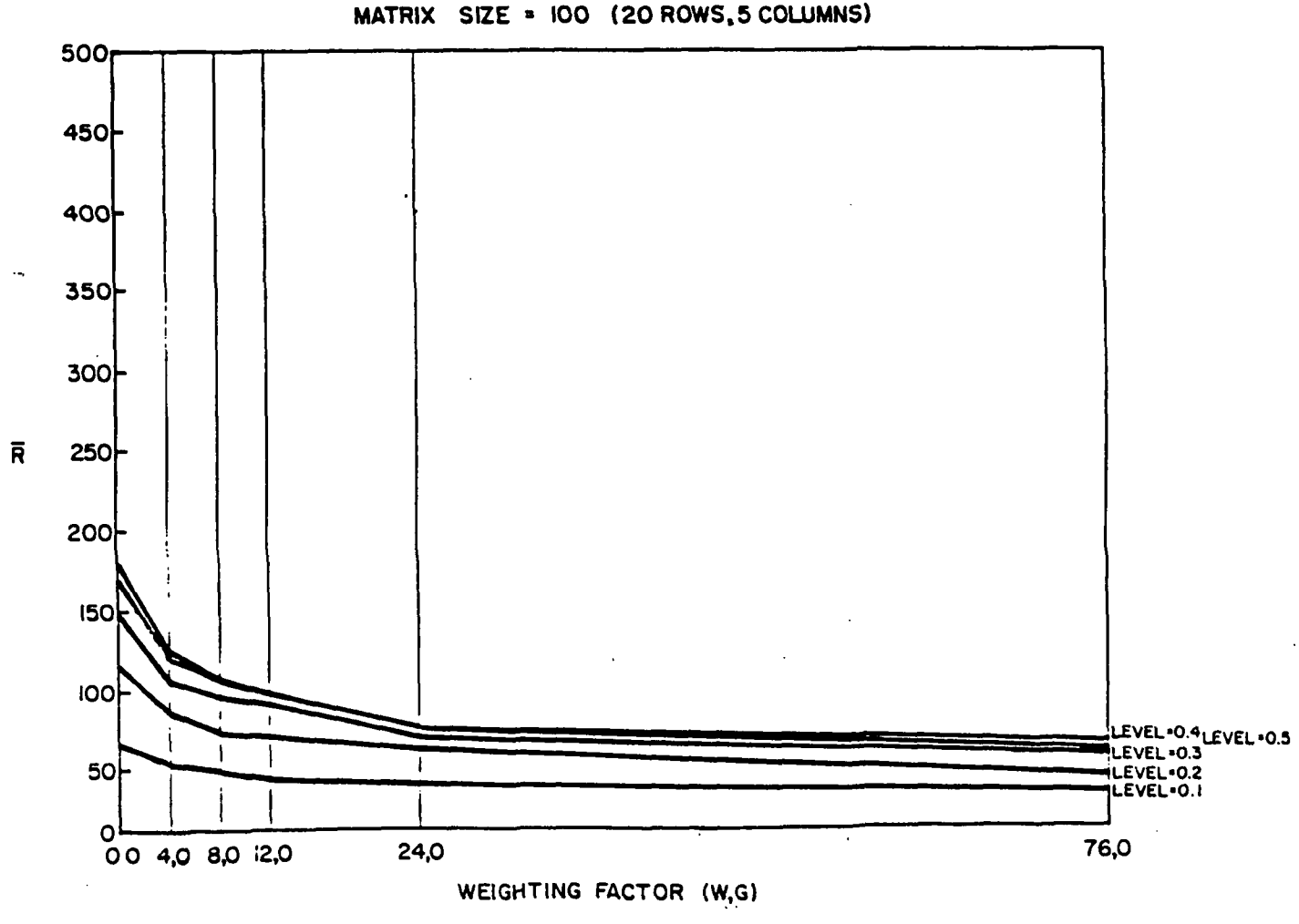

Figure 12. Plot of R-mean vs. weighting factors W and G = 0 for a 100-pixel matrix at five levels of disintegration.

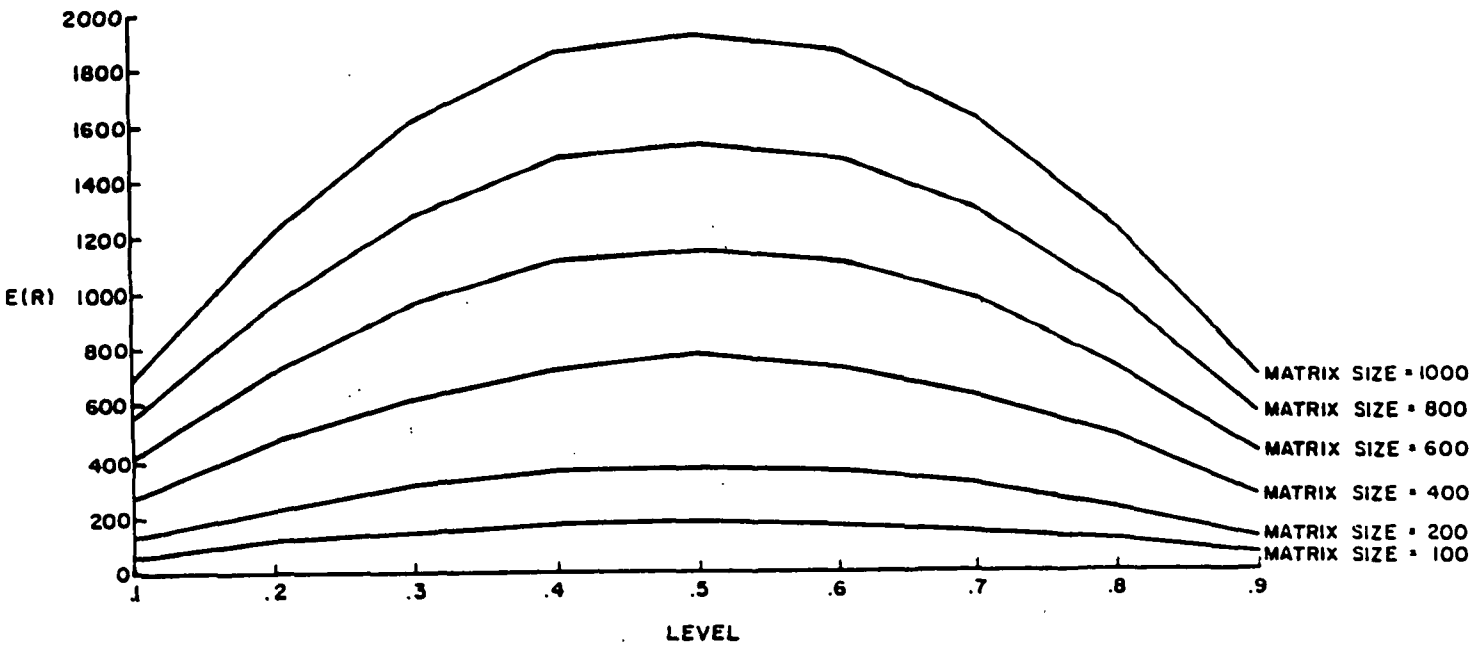

Figure 13. Plot of the expected value of the cross-product statistic, E(R), vs. level of disintegration for matrices of six different sizes (number of pixels).

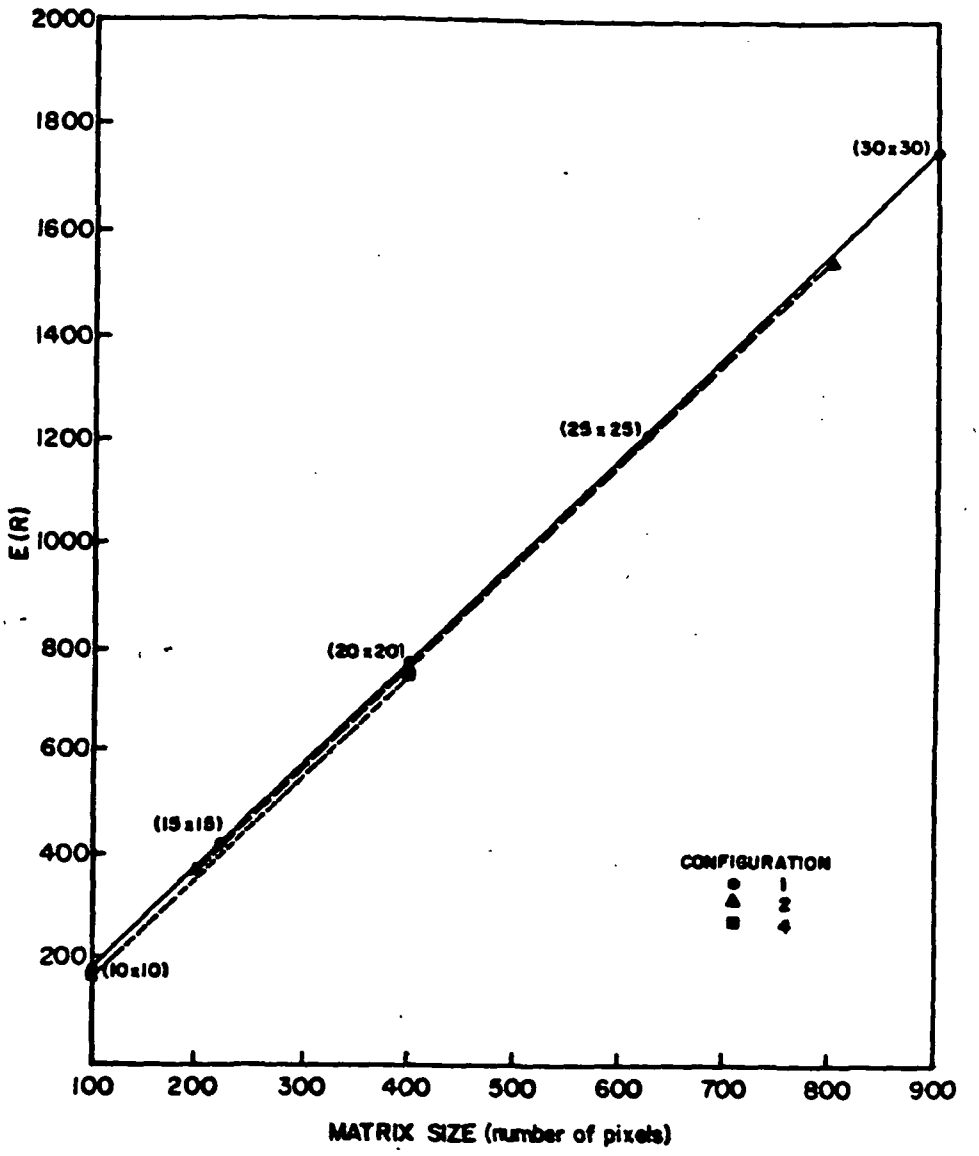

Figure 14. Plot of the expected value of the cross-product statistic, E(R), vs. matrix size (number of pixels) for matrices of the same configuration (ratio of rows to columns or the inverse).

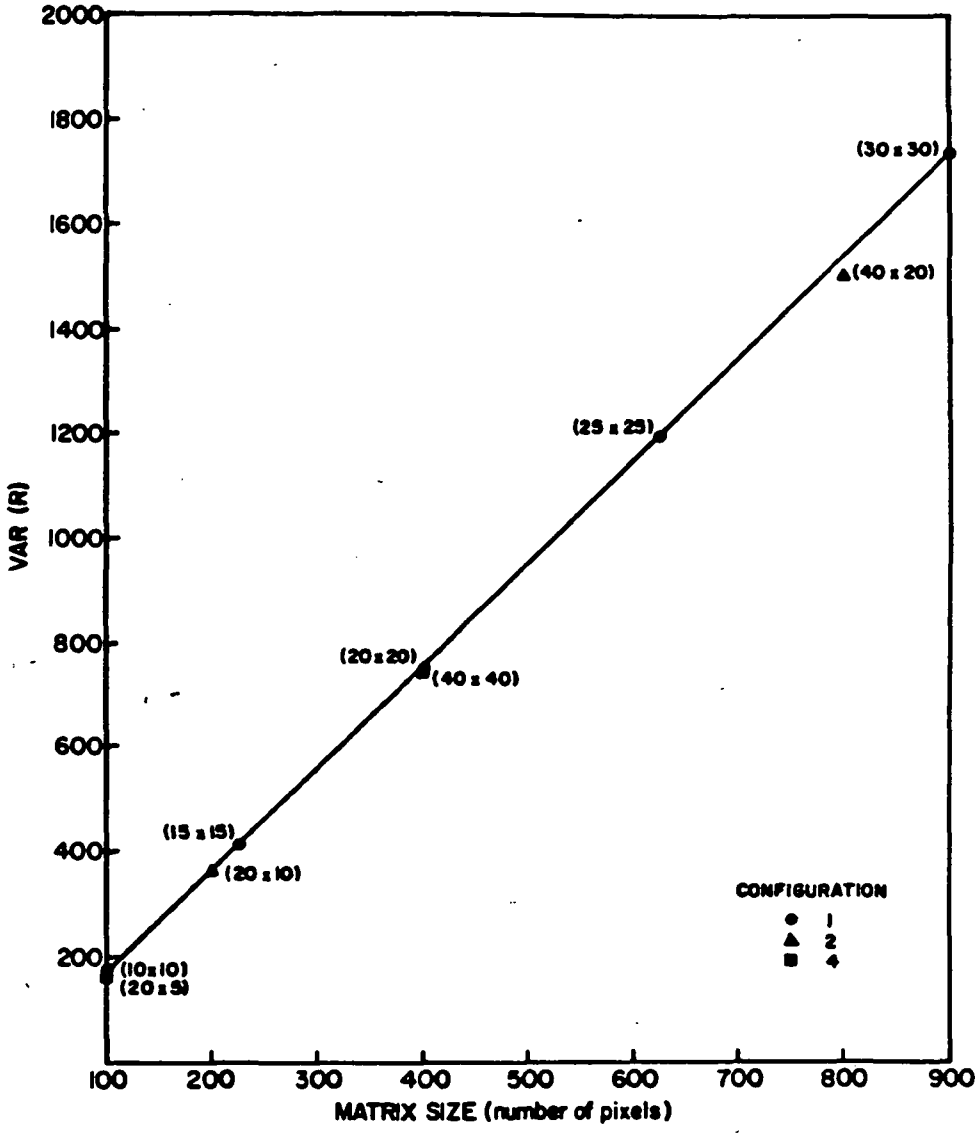

Figure 15. Plot of the variance of the cross-product statistic, var(R), vs. matrix size (number of pixels).

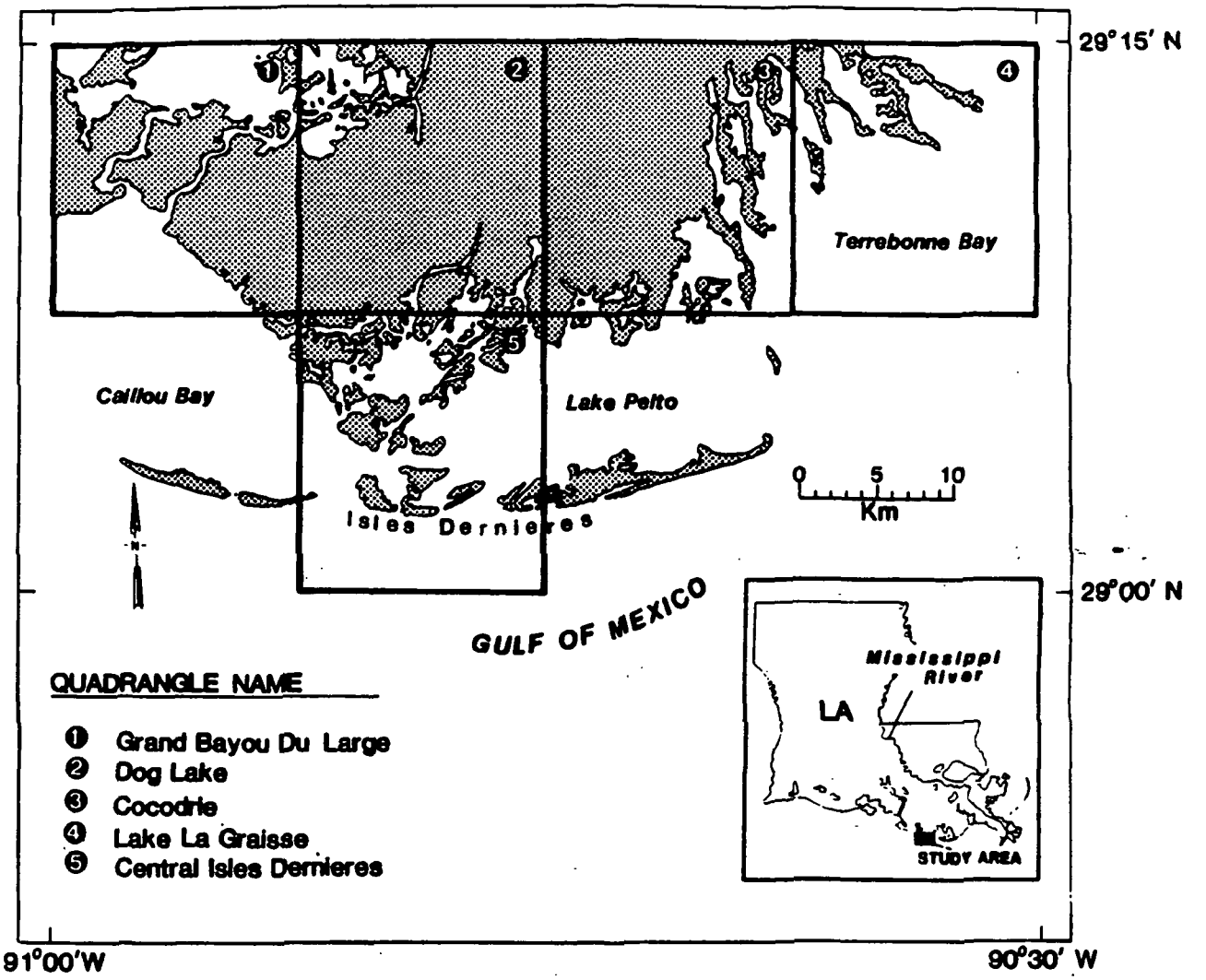

Figure 16. Location of the sample sites in Southeastern Louisiana.

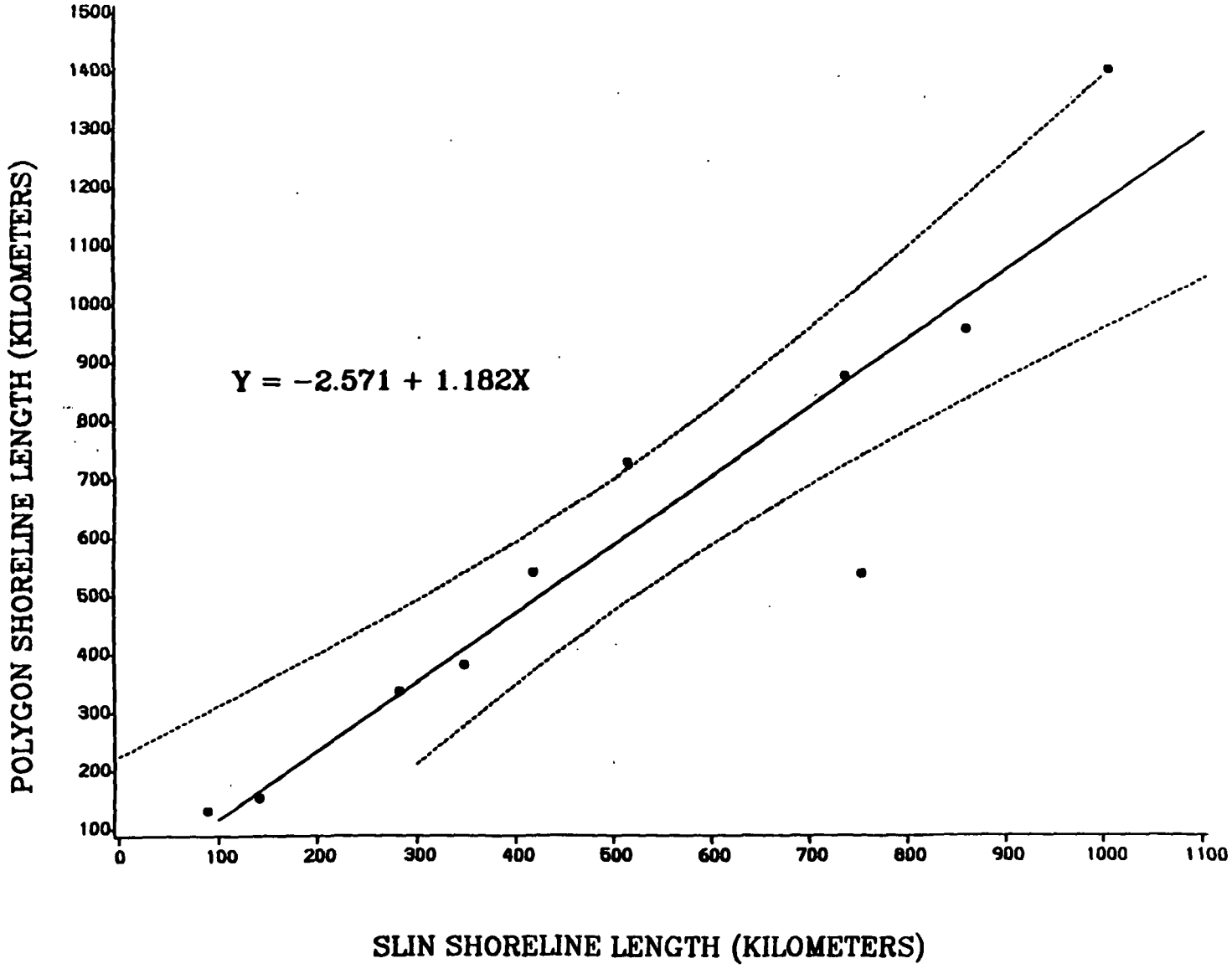

Figure 17. Regression of polygon shoreline lengths on SLIN shoreline lengths with 95% confidence limits for 1956 and 1978 USFWS habitat maps of the study area.

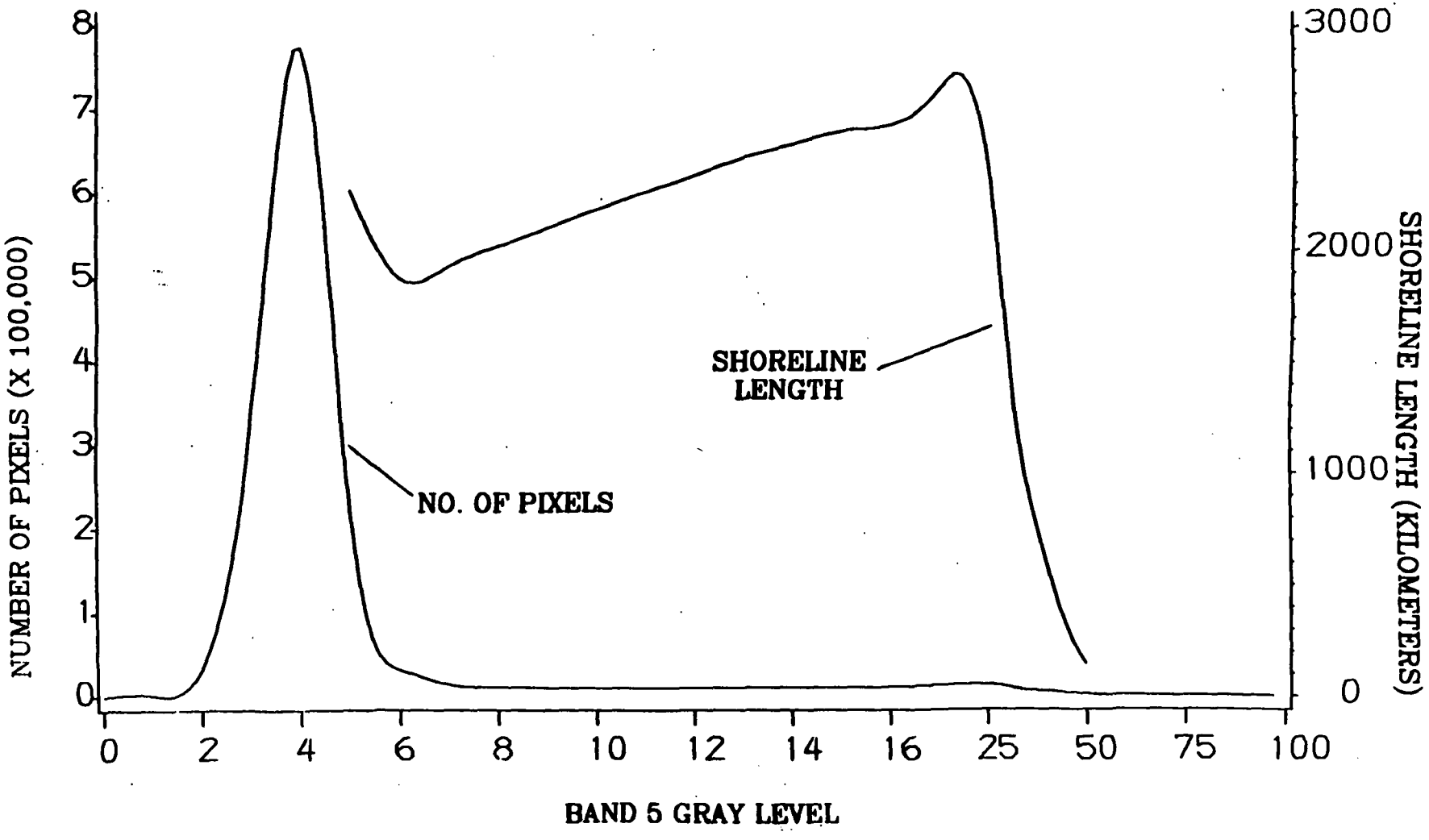

Figure 18. Relationship between the gray-level threshold and shoreline lengths from the band-5 image of the study sites.

Appendix Table 1 E(R) and VAR(R) as a function of level and R-mean and sample variance as a function of level and weighting factors for Matrix size = 1000 (20 rows, 50 columns)

E(R)

Level .1	.2	.3	.4	.5
695.50	1236.44	1622.82	1854.65	1931.93

VAR(R)

Level .1	.2	.3	.4	.5
277.60	816.95	1375.48	1779.91	1926.27

R-mean

Weights W,G	Level .1	.2	.3	.4	.5
0,0	700.60	1243.60	1619.80	1873.50	1948.80
4,4	554.93*	918.00*	1144.93*	1274.60*	1298.10*
8,8	503.66	808.80	1006.73	1097.80	1145.70
12,12	469.00	746.20	908.00	1028.53	1048.70
24,24	401.73	638.93	774.47	879.53	896.60
76,76	302.06	473.93	590.53	635.86	654.06

Sample variance

Weights W,G	Level .1	.2	.3	.4	.5
0,0	232.54	883.97	1493.76	1114.18	1347.07
4,4	396.78	1223.73	1759.21	3010.93	2560.85
8,8	425.48	1124.04	2754.44	2313.39	3985.49
12,12	456.87	1851.10	2060.61	2884.95	3773.62
24,24	652.46	1517.41	3814.80	3541.75	3385.53
76,76	684.48	2410.87	3594.60	3073.83	6561.84

*alpha risk < .001

Appendix Table 2 E(R) and VAR(R) as a function of level and R-mean and sample variance as a function of level and weighting factors for Matrix size = 800 (20 rows, 40 columns)

E(R)

Level

.1	.2	.3	.4	.5
559.09	986.83	1295.22	1480.25	1541.93

VAR(R)

Level

.1	.2	.3	.4	.5
222.83	652.99	1097.81	1419.79	1536.28

R-mean

Level

Weights W,G	.1	.2	.3	.4	.5
0,0	553.73	995.93	1288.33	1463.33	1553.73
4,4	447.53	729.80	903.47	1014.40	1037.60
8,8	396.40	646.73	800.93	914.93	922.33
12,12	363.87	597.80	725.53	812.13	829.00
24,24	317.60	505.67	622.67	700.27	718.60
76,76	252.40	390.73	471.27	520.80	526.47

Sample variance

Level

.1	.2	.3	.4	.5
178.26	414.60	1162.61	981.84	784.62
401.49	849.24	1928.03	1586.35	1617.04
595.49	671.68	1591.71	1673.67	2754.44
480.28	1270.96	2578.79	1764.16	4313.49
850.39	930.76	2058.82	1852.79	2190.23
617.77	2668.43	1604.42	2743.10	3841.57

Appendix Table 3 E(R) and VAR(R) as a function of level and R-mean and sample variance as a function of level and weighting factors for Matrix size = 600 (20 rows, 30 columns)

E(R)

Level

.1	.2	.3	.4	.5
414.69	737.23	967.61	1105.84	1151.92

VAR(R)

Level

.1	.2	.3	.4	.5
168.01	488.98	820.18	1059.68	1146.31

R-mean

Level

Weights W,G	.1	.2	.3	.4	.5
0,0	418.27	733.93	967.13	1106.67	1143.07
4,4	331.93	543.27	678.07	757.40	798.33
8,8	295.67	475.53	593.27	663.20	691.33
12,12	274.80	441.73	551.20	608.93	622.00
24,24	235.60	386.60	467.53	527.47	537.00
76,76	186.40	279.20	355.60	397.13	419.27

Sample variance

Level

.1	.2	.3	.4	.5
94.55	584.51	1391.46	1305.54	1051.42
263.17	690.15	882.80	1062.29	1441.78
306.27	826.47	1819.09	1443.28	1475.58
585.93	1120.75	872.32	2243.00	2706.15
421.84	958.56	1099.13	2290.75	2043.68
285.31	876.39	2407.00	2646.13	2311.50

Appendix Table 4 E(R) and VAR(R) as a function of level and R-mean and sample variance as a function of level and weighting factors for Matrix size = 400 (20 rows, 20 columns)

E(R)

Level

.1	.2	.3	.4	.5
274.29	487.62	640.00	731.43	761.90

VAR(R)

Level

.1	.2	.3	.4	.5
113.07	324.85	542.47	699.58	756.37

R-mean

Level

Weights W,G	.1	.2	.3	.4	.5
0,0	273.07	487.13	633.33	730.07	759.33
4,4	220.53	359.07	444.40	499.33	513.07
8,8	193.07	317.40	394.67	449.60	449.47
12,12	185.40	302.93	360.53	407.73	432.13
24,24	155.40	246.53	308.47	347.00	354.33
76,76	123.67	178.40	222.20	254.40	277.27

Sample variance

Level

Weights W,G	.1	.2	.3	.4	.5
0,0	130.52	329.41	587.36	780.77	488.94
4,4	234.94	529.30	845.23	584.51	1458.26
8,8	194.36	641.95	612.41	1129.99	1243.76
12,12	238.57	568.92	1570.73	780.77	1346.35
24,24	283.65	707.83	1325.51	1572.29	1627.34
76,76	289.31	1101.09	1121.41	1979.31	1420.95

Appendix Table 5 E(R) and VAR(R) as a function of level and R-mean and sample variance as a function of level and weighting factors for Matrix size = 200 (20 rows, 10 columns)

E(R)

Level

.1	.2	.3	.4	.5
133.87	237.99	312.36	356.98	371.86

VAR(R)

Level

.1	.2	.3	.4	.5
57.60	160.23	264.52	339.49	366.54

R-mean

Level

Weights W,G	.1	.2	.3	.4	.5
0,0	134.73	239.80	311.93	356.40	373.27
4,4	105.47	175.87	216.13	251.80	253.20
8,8	97.67	157.67	196.60	215.53	226.67
12,12	89.87	141.60	182.27	201.53	199.60
24,24	80.47	120.20	150.13	165.87	174.47
76,76	61.07	87.93	112.80	132.93	125.27

Sample variance

Level

.1	.2	.3	.4	.5
41.98	214.03	272.18	369.84	267.98
107.18	190.82	345.30	509.58	931.96
117.39	240.09	208.88	338.75	657.49
80.75	211.16	344.93	544.80	740.10
141.99	423.86	602.71	476.41	743.32
124.08	575.04	437.33	680.89	914.04

Appendix Table 6 E(R) and VAR(R) as a function of level and R-mean and sample variance as a function of level and weighting factors for Matrix size = 100 (20 rows, 5 columns)

E(R)

Level

.1	.2	.3	.4	.5
63.64	113.13	148.48	169.70	176.77

VAR(R)

Level

.1	.2	.3	.4	.5
28.65	76.79	125.03	159.51	171.93

R-mean

Level

Weights W,G	.1	.2	.3	.4	.5
0,0	63.67	114.33	148.07	170.93	177.87
4,4	52.47	80.00	105.53	116.13	118.13
8,8	47.60	76.33	90.60	100.07	101.67
12,12	42.53	71.47	83.20	92.87	94.47
24,24	37.00	60.80	72.13	78.00	78.47
76,76	28.67	43.80	52.60	58.33	56.67

Sample variance

Level

.1	.2	.3	.4	.5
37.88	69.67	98.60	137.58	170.22
44.69	64.20	158.62	197.39	218.66
38.24	101.95	148.87	135.97	244.69
48.72	139.20	206.61	288.31	339.11
81.81	104.35	269.59	196.56	278.05
65.63	218.37	224.81	307.65	287.97

Appendix Table 7 E(R) and VAR(R) as a function of level and R-mean and sample variance as a function of level and weighting factors for Matrix size = 1000 (20 rows, 50 columns)

E(R)

Level				
.1	.2	.3	.4	.5
695.50	1236.44	1622.82	1854.65	1931.93

VAR(R)

Level				
.1	.2	.3	.4	.5
277.60	816.95	1375.48	1779.91	1926.27

R-mean

Weights W,G	Level				
	.1	.2	.3	.4	.5
0,0	700.60	1243.60	1619.80	1873.50	1948.80
4,0	562.60*	926.06*	1147.47*	1281.86*	1305.86*
8,0	517.67	822.66	1026.60	1123.33	1148.00
12,0	474.67	756.13	928.80	1043.66	1078.06
24,0	426.80	660.33	829.27	892.60	895.26
76,0	328.60	516.13	614.60	658.33	703.53

Sample variance

Weights W,G	Level				
	.1	.2	.3	.4	.5
0,0	232.54	883.97	1493.76	1114.18	1347.07
4,0	524.79	1015.39	1898.78	2041.91	2486.76
8,0	334.06	1301.99	2215.15	3016.32	3278.83
12,0	476.41	1569.95	1420.21	2737.95	4019.08
24,0	751.92	1462.76	2411.83	5818.03	5526.30
76,0	1254.19	1465.77	3402.71	3182.71	4303.17

*alpha risk < .001

Appendix Table 8 E(R) and VAR(R) as a function of level and R-mean and sample variance as a function of level and weighting factors for Matrix size = 800 (20 rows, 40 columns)

E(R)

Level

.1	.2	.3	.4	.5
559.09	986.83	1295.22	1480.25	1541.93

VAR(R)

Level

.1	.2	.3	.4	.5
222.83	652.99	1097.81	1419.79	1536.28

R-mean

Level

Weights W,G	.1	.2	.3	.4	.5
0,0	553.73	995.93	1288.33	1463.33	1553.73
4,0	456.33	747.27	927.33	1030.93	1041.60
8,0	404.60	658.80	825.93	903.33	912.13
12,0	373.80	614.07	760.93	841.87	862.93
24,0	329.20	536.87	674.40	714.20	734.53
76,0	272.13	415.00	478.53	552.13	552.13

Sample variance

Level

.1	.2	.3	.4	.5
178.26	414.60	1162.61	981.84	784.62
298.07	672.19	1008.51	1311.94	2136.27
346.03	975.68	1091.97	2004.76	2574.80
679.35	1398.07	1488.45	2135.36	1532.00
643.95	1143.91	1336.99	2846.00	2582.79
519.85	1178.75	2048.13	2439.92	3186.04

Appendix Table 9 E(R) and VAR(R) as a function of level and R-mean and sample variance as a function of level and weighting factors for Matrix size = 600 (20 rows, 30 columns)

E(R)

Level

.1	.2	.3	.4	.5
414.69	737.23	967.61	1105.84	1151.92

VAR(R)

Level

.1	.2	.3	.4	.5
168.01	488.98	820.18	1059.68	1146.31

R-mean

Level

Weights W,G	.1	.2	.3	.4	.5
0,0	418.27	733.93	967.13	1106.67	1143.07
4,0	338.13	552.27	681.47	757.60	768.53
8,0	308.93	490.40	608.13	670.27	692.53
12,0	285.13	462.60	567.07	622.27	649.40
24,0	251.07	385.47	478.60	526.40	545.80
76,0	185.87	300.67	376.73	415.27	422.73

Sample variance

Level

.1	.2	.3	.4	.5
94.55	584.51	1391.46	1305.54	1051.42
208.03	811.84	1317.65	1274.46	1617.04
352.28	446.01	978.76	1571.51	2397.37
223.92	1135.28	1664.03	2000.36	1697.08
432.41	1043.78	1790.69	1919.40	2271.96
552.63	667.10	1978.43	1654.42	2732.81

Appendix Table 10 E(R) and VAR(R) as a function of level and R-mean and sample variance as a function of level and weighting factors for Matrix size = 400 (20 rows, 20 columns)

E(R)

Level

.1	.2	.3	.4	.5
274.29	487.62	640.00	731.43	761.90

VAR(R)

Level

.1	.2	.3	.4	.5
113.07	324.85	542.47	699.58	756.37

R-mean

Level

Weights W,G	.1	.2	.3	.4	.5
0,0	273.07	487.13	633.33	730.07	759.33
4,0	225.00	365.93	447.60	514.27	504.73
8,0	204.81	322.60	392.87	442.73	460.53
12,0	189.07	298.67	374.80	408.93	420.53
24,0	174.00	263.27	318.13	369.40	368.80
76,0	131.60	204.40	238.07	267.73	278.87

Sample variance

Level

.1	.2	.3	.4	.5
130.52	329.41	587.36	780.77	488.94
197.67	418.62	821.96	495.48	1316.93
308.69	552.16	1070.63	774.74	1101.09
284.98	689.12	576.93	1088.73	1495.28
196.29	516.71	1014.14	1418.73	972.00
370.97	898.65	809.04	1236.84	900.42

Appendix Table 11 E(R) and VAR(R) as a function of level and R-mean and sample variance as a function of level and weighting factors for Matrix size = 200 (20 rows, 10 columns)

E(R)

Level

.1	.2	.3	.4	.5
133.87	237.99	312.36	356.98	371.86

VAR(R)

Level

.1	.2	.3	.4	.5
57.60	160.23	264.52	339.49	366.54

R-mean

Level

Weights W,G	.1	.2	.3	.4	.5
0,0	134.73	239.80	311.93	356.40	373.27
4,0	112.53	180.40	226.20	244.07	248.27
8,0	99.87	158.47	190.33	219.13	221.93
12,0	96.80	141.13	185.27	203.13	197.80
24,0	85.33	127.53	157.67	179.27	171.93
76,0	67.20	102.87	119.60	133.40	128.73

Sample variance

Level

.1	.2	.3	.4	.5
41.98	214.03	272.18	369.84	267.98
58.06	145.06	449.75	461.50	348.23
80.22	200.72	454.77	495.48	467.86
64.20	205.49	244.38	461.08	367.57
99.58	172.79	443.52	439.80	311.46
145.53	204.36	543.42	649.95	818.02

Appendix Table 12 E(R) and VAR(R) as a function of level and R-mean and sample variance as a function of level and weighting factors for Matrix size = 100 (20 rows, 5 columns)

E(R)

Level

.1	.2	.3	.4	.5
63.64	113.13	148.48	169.70	176.77

VAR(R)

Level

.1	.2	.3	.4	.5
28.65	76.79	125.03	159.51	171.93

R-mean

Level

Weights W,G	.1	.2	.3	.4	.5
0,0	63.67	114.33	148.07	170.93	177.87
4,0	51.53	85.40	104.53	118.07	119.73
8,0	48.20	73.13	93.27	104.67	105.87
12,0	43.73	71.40	90.27	94.93	95.27
24,0	41.00	62.27	70.80	75.27	74.67
76,0	35.07	47.20	59.60	65.20	61.40

Sample variance

Level

.1	.2	.3	.4	.5
37.88	69.67	98.60	137.58	170.22
34.80	95.70	189.73	212.59	219.53
60.32	103.55	180.90	172.79	303.53
26.34	69.34	242.23	158.13	449.43
47.09	151.76	139.89	348.96	325.85
48.72	99.00	289.31	372.87	818.02